2024

# Mid-21St Century Chesapeake Bay Hypoxia: The Role Of Climate Change At The Atmospheric, Terrestrial, And Oceanic Boundaries

Colin Hawes
*College of William and Mary - Virginia Institute of Marine Science*, hawes714@gmail.com

# Mid-21st Century Chesapeake Bay Hypoxia: The Role of Climate Change at the Atmospheric, Terrestrial, and Oceanic Boundaries

A Thesis

Presented to

The Faculty of the School of Marine Science

The College of William and Mary in Virginia

In Partial Fulfillment

of the Requirements for the Degree of

Master of Science

by

Colin Ashton Hawes

August 2024

# APPROVAL PAGE

This thesis is submitted in partial fulfillment of

the requirements for the degree of

Master of Science

Colin Hawes

Approved by the Committee, August 2024

Marjorie A.M. Friedrichs, Ph.D.
Committee Chair / Advisor

Pierre St-Laurent, Ph.D.

Mary Fabrizio, Ph.D.

Piero Mazzini, Ph.D.

Raymond Najjar, Ph.D.
The Pennsylvania State University
State College, PA, USA

# TABLE OF CONTENTS

# ACKNOWLEDGEMENTS

It is most important that I sincerely thank my advisor, Dr. Marjy Friedrichs. My appreciation for your support, while I have been exploring the field of numerical modeling, learning its many applications and forming my career goals, can not be understated. Thank you for ardently providing me with unique opportunities and invaluable guidance. With the knowledge I have gained, I excitedly look forward to the new problems I will face.

Thank you to Dr. Pierre St-Laurent for taking the time to clearly explain and discuss so many of the interesting fine details of numerical modeling. Thank you to Dr. Mary Fabrizio, Dr. Piero Mazzini, and Dr. Raymond Najjar. I appreciate all the times you have each checked in on me to provide feedback and encouragement. To all my committee, thank you for asking me questions I would have otherwise never thought to seek answers to.

Moving to Williamsburg and joining the VIMS community in the spring of 2021 was difficult, but the members of the BioCOM lab made it much easier. Thank you, Dr. Jessie Turner and Luke Frankel, for making me feel welcome. Thank you, Dr. Fei Da and Dr. Kyle Hinson, for being amazing mentors throughout my first few years. Thank you, Catherine Czajka, for being there through the whole process with wise advice and invitations to YROC. Thank you, Alexa Labossiere and Olivia Szot, seeing both of your work has been inspiring. Thank you to Dr. Dante Horemans for your feedback and discussion both in and out of lab meetings.

Thank you, Mom, Dad and Emma, for supporting my journey and always being there with the promise (threat) of foam #1 fingers at my presentations. Mo, thank you for all your love as we navigated a relationship formed during a pandemic, serendipitously chose the same university, and supported each others pursuit of our careers.

A special thank you to my best friend Colin Carrol for his enduring patience with me.

This research was also greatly improved by help of additional collaborators from Penn State (Ray Najjar and Maria Herrmann), the Chesapeake Bay Program Office (Gary Shenk, Gopal Bhatt, Lewis Linker, Richard Tian, and Isabella Bertani), Old Dominion (Eileen Hofmann), and Auburn University (Zihao Bian, Yuanzhi Yao, and Hanqin Tian). I greatly appreciate their feedback as well as all the prior and concurrent work they conducted which provided key input forcings for my runs.

Thank you to the HPC support team and maintenance crews at VIMS and William & Mary whose work supported the computing power necessary to conduct this research. Lastly, thank you to all the current and former administrative staff who have helped me navigate the logistics of graduate life, conference travel, and funding: Gina Burrell, Maxine Butler, Cathy Cake, Jen Hay, Linda Schaffner, John Griffin, and VIMS GSA.

# ABSTRACT

Climate change is already increasing the volume and duration of coastal hypoxia and threatening living resources, particularly in eutrophic ecosystems. Atmospheric warming exacerbates deoxygenation by decreasing gas solubility and enhancing respiration and remineralization. Changes in terrestrial runoff and sea level influence hypoxia via nutrient availability and altered water temperature, respectively. However, the impacts of other future climate changes, including winds, shortwave and longwave radiation, non-runoff precipitation, and ocean water conditions, are still unknown. In this study, the impacts of such future climate changes on hypoxia in Chesapeake Bay were examined using a 3-D coupled estuarine hydrodynamic–biogeochemical model linked to a regulatory watershed model. A control run simulated 1991-1995; while mid-21$^{st}$ century projections assuming no change in management actions were generated by applying downscaled outputs of three Earth System Models (ESMs), run under a "business as usual" emissions scenario. Mid-21$^{st}$ century hypoxic volume ($O_2$ < 3 mg $L^{-1}$) integrated over all days of a given year, also called annual hypoxic volume (AHV), is projected to increase by a minimum of 13% up to a maximum of 35%, when using the centroid ESM, with higher freshwater discharge years resulting in smaller percent increases. The use of future climate projections from the other two ESMs resulted in five-year average percent increases in AHV of 5% (relatively cool and dry ESM), 21% (centroid ESM) and 35% (relatively hot and wet ESM). Future changes to hypoxia are projected to vary seasonally, with hypoxic conditions projected to start earlier, but no change or decreased hypoxia in mid-summer. Finally, model runs with subsets of modified climate forcings revealed that air temperature accounted for the majority (72 ± 18%, five-year mean ± standard deviation) of the increase in AHV. Next most impactful to AHV were climate changes to watershed inputs (21 ± 31%) and sea level (-1 ± 24%), with both impacts being highly dependent on freshwater discharge. Finally, changes to winds, radiation, non-runoff precipitation, and ocean water conditions cumulatively accounted for only small future percent increases in AHV (5 ± 3%). To reach regulatory water quality goals despite these competing impacts of climate change, future nutrient management actions will likely need to be more aggressive.

# Mid-21st Century Chesapeake Bay Hypoxia: The Role of Climate Change at the Atmospheric, Terrestrial, and Oceanic Boundaries

# 1 INTRODUCTION

Across the globe, hypoxia in coastal eutrophic ecosystems is impacted by the growing pressures of climate change. Despite differences in physical and biogeochemical characteristics, water bodies such as the Chesapeake Bay, the Gulf of Mexico, the Baltic Sea, and Long Island Sound (Bianchi et al., 2010; Staniec and Vlahos, 2017; L. Slater et al., 2020; Viitasalo and Bonsdorff, 2022) each face reduced habitat volume, decreased biodiversity, and altered food-web interactions due to coastal hypoxia (Diaz and Rosenberg, 2008). Higher trophic level organisms may die off when squeezed between excessively warm waters at the surface and hypoxia at the bottom (Breitburg, 2002). Food-web interactions may be altered as hypoxic habitats are used by some species as a refuge from predation (Hedges and Abrahams, 2015; Crear et al., 2020). When projecting future spatial and temporal changes to living resources, hypoxia will be a key stressor not only due to how it may alter food-web dynamics, but also due to its impacts on physiological conditions like reproductive tissue and metabolic rates (Tuckey and Fabrizio, 2016; Slesinger et al., 2019).

Historically, a leading cause of increasing coastal hypoxia has been excessive anthropogenic nutrient loading (Diaz and Rosenberg, 2008), but climate change impacts such as increasing temperatures and altered precipitation patterns are increasingly exacerbating the volume and duration of coastal hypoxia (Leal Filho et al., 2022; Hao et al., 2024; Hinson et al., 2024). It is less clear whether other impacts of future climate, such as changes in wind and radiation, may also affect future hypoxia. Because local ecosystem managers cannot directly reduce global climate change, they typically focus on improving water quality by reducing nutrient loads (McCrackin et al., 2017; Hood et al., 2021; Frankel et al., 2022; Bhatt et al., 2023).

To successfully counter the predicted future impacts of climate change on coastal hypoxia, the potential impacts of those less studied variables, like radiation, need to be well understood.

The Chesapeake Bay is the largest estuary in the continental U.S. and is a prime example of a system which is managed by nutrient reductions while simultaneously being impacted by changes in climate (Linker et al., 2024). This estuarine system is naturally eutrophic, so some degree of seasonal hypoxia is expected (Kemp et al., 2005). However, in the 1980s and 1990s increasingly large nutrient loads from human activity fueled the biological chain of eutrophication resulting in more intense and prolonged periods of hypoxia. In more recent years, nutrient reductions have been decreasing hypoxia in the Bay (Frankel et al., 2022). However, recent estuarine warming (Hinson et al., 2022) is increasing rates of microbial respiration and decreasing gas solubility (Du et al., 2018; Irby et al., 2018), which counteract the improvements due to management actions (Ni et al., 2020; Frankel et al., 2022).

Other impacts of climate change on Chesapeake Bay hypoxia are less clear. For example, it has been suggested that sea level rise may increase bottom oxygen ($O_2$) concentrations through enhanced gravitational circulation inputting more $O_2$-rich water to the lower depth layers of the Bay (Wang et al., 2017; Cai et al., 2022). Another explanation is that sea level rise may increase bottom $O_2$ in early because the deeper Bay waters take longer to warm at the start of the hypoxic season (St-Laurent et al., 2019). Changes in terrestrial runoff may also impact hypoxia by affecting future streamflow and the delivery of nutrients to the estuary. While future precipitation and terrestrial runoff projections have large uncertainties, there is evidence that although overall precipitation over the watershed may increase by mid-century, terrestrial freshwater runoff may decrease because of the effect of increased evapotranspiration due to higher temperatures (Bhatt et al., 2023). However, storm intensity and Susquehanna River winter streamflow are projected

to increase in the future (Bhatt et al., 2023; Linker et al., 2024), leading to complex impacts on future hypoxia. Other potentially important but less well-studied mechanisms for impacting future hypoxia include changing shortwave and longwave radiation, winds, non-runoff precipitation over Bay water, and water conditions on the continental shelf. This study aims to further investigate the relative magnitude of the impacts of these processes on mid 21$^{st}$ century hypoxia and understand how these impacts may vary depending on hydrological conditions.

When estimating future hypoxia, one of the largest sources of uncertainty is the climate projection chosen for future atmospheric conditions (Hinson et al., 2023). Early Chesapeake Bay modeling studies used sensitivity analyses (Irby et al., 2018) or a single climate projection (an average of six Earth System Models, ESMs, Wang et al., 2017) to examine the impact of future climate on hypoxia. However, the applicability of these future projections to management decisions was limited, as the full extent of future climate variability was not assessed. In the Chesapeake Bay, later studies (Ni et al., 2019; Hinson et al., 2023) have used multiple ESM projections in their model runs, and found a large sensitivity to ESM choice. However, these studies only examined a subset of future climate change variables and did not fully address the impact of interannual variability on future hypoxia estimates. Furthermore, studies in other estuarine systems that have used more comprehensive sets of changed climate variables haven't examined the impacts on hypoxia of changing each climate variable in isolation (Hafeez et al., 2021; Huggett et al., 2021), which would give insight into the prioritization of management actions. In this study, regionally downscaled outputs of multiple ESMs were used to investigate future climate change impacts, including air temperature, sea level rise, terrestrial runoff, winds, shortwave and longwave radiation, direct precipitation on the Bay, and coastal ocean changes. The results, including information on both high run-off and low run-off years, can provide

critical information to Chesapeake Bay managers to help them consider the impacts of a complete set of changing environmental parameters.

## 2 METHODS

### 2.1 Chesapeake Bay model

The numerical model used in this study is a fully coupled hydrodynamic–biogeochemical system (Feng et al., 2015). It includes a 3-D Estuarine Carbon and Biogeochemistry (ECB) model embedded within the Regional Ocean Modeling System (ROMS; Shchepetkin and McWilliams, 2005) and is hereafter referred to as ROMS-ECB. The model grid includes, for all 20 terrain-following vertical levels, the full Bay and its tributaries, as well as a portion of the mid-Atlantic Bight on the continental shelf (Fig. 1). Along with the physical state variables included in ROMS, the ECB model includes the following biogeochemical state variables: nitrate, ammonium, phytoplankton, zooplankton, small and large detrital nitrogen, semilabile and refractory DON, small and large detrital carbon, semilabile and refractory dissolved organic carbon (DOC), and $O_2$. Following Turner et al. (2021), there are four suspended sediment size classes simulated with settling velocities typical of sand, silt-rich flocs, clay-rich flocs and unaggregated mud. The water column concentrations of these sediment size classes impacts light attenuation and thus primary productivity, which is a key source of $O_2$ in the model.

The version of ROMS-ECB used here is an update from that used in several recent publications (St-Laurent et al., 2020; Frankel et al., 2022; Hinson et al., 2024). Updates, as recently described in St-Laurent and Friedrichs (2024), include a higher resolution grid with a horizontal resolution of 600 × 600 m, more spatially distributed watershed inputs (83 locations; Fig. 1), as well as wetting and drying, which allows cells to alternate between wet and dry states

in the shallow reaches of the Bay. Additionally, the growth function of the phytoplankton state variable was updated to include a Michaelis-Menten parameterization for salinity, with a half-saturation constant of 2.5. This was updated because the phytoplankton is parameterized to be representative of marine algal taxa. Freshwater algal taxa are implicitly represented in ECB as part of the terrestrial inputs of organic matter. To improve the model's skill in reproducing nutrient and oxygen concentrations, the parameters defining the solubilization rate of large and small detrital nitrogen and carbon into DON and DOC at 0 °C were set to 0.09 $d^{-1}$, and those parameters defining the remineralization of DON and DOC at 0 °C were set to 0.01 $d^{-1}$. The change in these parameters affects all temperatures, not just 0 °C. In addition, the minimum temperature-dependent phytoplankton growth rate and the growth rate coefficient from Hinson et al. (2024) were respectively increased to 3.5 $d^{-1}$ and 0.55 $d^{-1}$. Finally, the ballasting parameterization of Turner et al. (2021) was included such that sinking rates are higher as organic and inorganic particles aggregate.

### 2.2 1991-1995 Reference simulation

A "Reference" simulation was run for the years 1991-1995. This time period was chosen because it occurs before many management actions were implemented, and is the reference time frame used by the Chesapeake Bay Program for their nutrient management scenarios (Bhatt et al., 2023; Linker et al., 2024). This period includes a variety of high and low runoff years. While the average total discharge (± standard deviation) to the Bay over 1985-2020 is 73 ± 20 $km^3$ $y^{-1}$, the five reference years are characterized by the following freshwater discharges: 1991: 52 $km^3$ $y^{-1}$, 1992: 60 $km^3$ $y^{-1}$, 1993: 87 $km^3$ $y^{-1}$, 1994: 87 $km^3$ $y^{-1}$, and 1995, 55 $km^3$ $y^{-1}$. Daily average summer (May through September) air temperatures averaged over the Bay for these five years

were: 1991: 23.2 °C, 1992: 21.2 °C, 1993: 22.8 °C, 1994: 22.1 °C, and 1995: 22.6 °C; with a 1985-2020 Bay average summer air temperature of 22.6 ± 0.7 °C.

**2.2.1** ***1991-1995 atmospheric forcing.*** The Reference simulation was forced at the surface-air boundary by the European Centre for Medium-Range Weather Forecasts fifth generation global atmospheric reanalysis products (ERA5; Hersbach et al., 2020). The ERA5 products (2-meter air temperature, net shortwave radiation, downwelling longwave radiation, wind speed, wind direction, and precipitation; Table 1) have a horizontal resolution of 0.25° and were implemented with a three-hourly time step. Relative humidity was calculated from surface air temperature and dewpoint temperature. Wet and dry atmospheric nitrate and ammonium deposition were also included, following Da et al. (2018).

**2.2.2** ***1991-1995 terrestrial forcing*****.** Daily terrestrial inputs were provided by the United States Environmental Protection Agency's (EPA's) regulatory Phase 6 Watershed Model (Phase 6; Bhatt et al., 2023). Daily forcings of point, non-point, and shoreline sources at 2,475 cells adjacent to the Bay were manually summed and mapped onto the 83 terrestrial input locations (Fig. 1). Direct or derived Phase 6 outputs provided forcings for freshwater mass transport, water temperature, $O_2$, nitrate, ammonium, semilabile and refractory DON, small and large detrital nitrogen, and four suspended sediment size classes (representing sand, silt-rich flocs, clay-rich flocs, and unaggregated mud). The nitrogen constituents of Phase 6 were redistributed to match the estuarine model, following Frankel et al. (2022), with the exception that, as in Hinson et al. (2023), the percent of refractory organic nitrogen assigned to the ROMS-ECB refractory DON state variable is assumed to increase with streamflow at high flow volumes. Carbon concentrations were not available directly from Phase 6, and therefore were derived from

their nitrogen counterparts assuming semilabile DOC:DON = 10, refractory DOC:DON = 17 (Hopkinson and Vallino, 2005), and assuming small detrital C:N = 6.625 (Redfield, 1934).

**2.2.3** ***1991-1995 continental shelf boundary conditions*****.** Reference conditions on the continental shelf boundary were obtained from Da et al. (2021) and included climatological temperature and salinity (Zweng et al., 2019). $O_2$ concentrations along the outer boundary were calculated from these temperature and salinity fields assuming saturation (Garcia and Gordon, 1992). Sea surface height on the continental shelf was calculated using tidal harmonics from the Advanced Circulation model (Luettich et al., 1992) and from hourly nontidal water level observations at stations in Duck, NC and Lewes, DE (Da et al., 2018). Outside sources of nitrogen from the open boundary were ignored.

## 2.3 Chesapeake Bay data

Physical and biogeochemical cruise data collected as part of the Chesapeake Bay Program's (CBP) Tidal Water Quality Monitoring Program (CBP Database, 2024) were used in this study to evaluate ROMS-ECB. Since 1984, the CBP has been recording water quality data during routine sampling at fixed stations throughout the Bay. Sampling occurs twice per month during warmer months, and once per month during colder months. At each station, vertical profiles of temperature, salinity, and oxygen ($O_2$) are available at 1 m intervals throughout the water column. Nitrate and dissolved organic nitrogen (DON) concentrations were measured at the surface and bottom of the water column, and in deeper waters data were also collected above and below the pycnocline. These data were used for model evaluation at 25 stations within the Bay's main stem and the Potomac tributary (Fig. 1). Data-based estimates of hypoxic volume are available from calculations using a volumetric inverse distance squared interpolator program (USEPA, 2003) applied to the WQMP profiles of $O_2$ (Bever et al., 2013, 2018).

## 2.4 Model skill

Model skill was assessed by calculating the root mean squared difference (RMSD) between the Reference simulation and available data from the CBP's WQMP described above. Hourly model output was matched with observations closest in space and time, and both means and standard deviations were compared. Specifically, model output at the surface and bottom levels were compared with observations at corresponding depths at 25 stations (Fig. 1) for the following variables: temperature, salinity, $O_2$, nitrate, and dissolved organic nitrogen. Lastly, hypoxic volume was computed from the Reference simulation for multiple $O_2$ thresholds (volume where $O_2$ < 1, 2, and 3 mg $L^{-1}$) and evaluated against data-based estimates of hypoxic volume calculated via the interpolation of observed $O_2$ profiles (Bever et al., 2018). Annual hypoxic volume (AHV), with units of $km^3$ d, is calculated as the integral of daily hypoxic volume throughout a year from both ROMS-ECB and the interpolated estimates. As discussed in Bever et al. (2013) and Bever et al. (2018), estimates of hypoxia from these two models are not expected to agree precisely.

## 2.5 Mid-21st century (2046-2050) model runs

Choosing a set of ESMs to force the estuarine model is important for estimating uncertainty in predicted future hypoxic conditions (Ni et al., 2019; Hinson et al., 2023). This is especially true for a future as early as the mid-21st century, when emissions scenarios are not yet predicted to diverge as much as by 2100 (Moss et al., 2010; Taylor et al., 2012). In this study atmospheric forcings for the mid-21st century (2046-2050) were obtained from regionally downscaled atmospheric components of three ESMs using a "business as usual" emissions scenario. Given this study's central goal of determining hypoxia's sensitivity to multiple future

climate conditions, Representative Concentration Pathway (RCP 8.5) was selected as being most informative.

Atmospheric forcings for the mid-21st century (2046-2050) were obtained from the regionally downscaled atmospheric components of three ESMs. As in Hinson et al. (2023), the Multivariate Adapted Constructed Analogs (MACA) technique (Abatzoglou and Brown, 2012) was used to provide statistically downscaled climate forcings at a 1/24º resolution. An advantage of MACA over other downscaling techniques commonly used is that multiple downscaled fields are available including winds, relative humidity, and shortwave radiation in addition to temperature and precipitation. However, the MACA downscaling does not include longwave radiation, a major component in the global surface heat budget. Following Herrmann and Najjar (2023), downwelling longwave radiation was estimated via an algorithm which required input variables of air temperature, shortwave radiation, and humidity (all available from the MACA downscaled products). Similarly to Ni et al. (2019) and Hinson et al. (2023), three ESMs selected from an ensemble of 20 ESMs, available from the Coupled Model Intercomparison Project (Taylor et al., 2012), using the Katsavounidis-Kuo-Zhang (KKZ) algorithm (Katsavounidis et al., 1994). KKZ incrementally selects a subset of models that best represent the ensemble's full range within a given multivariate space. Ross and Najjar (2019) applied the KKZ algorithm to select ESMs for use in watershed models to predict hydrologic change, and found that it was more effective at using the fewest ESMs to cover the largest range of outcomes compared to other selection algorithms. In this study, as in Hinson et al. (2023), ESMs were sorted by the expected greatest drivers of change in future hypoxia, specifically changes in air temperature from May-October and precipitation from November-June. The three ESMs selected via the KKZ algorithm for use in this study include the: Centroid (Cent.; Dufresne et al., 2013),

Cool/Dry (C/D; Volodin et al., 2010), and Hot/Wet (H/W; Martin et al., 2011). These represent a typical ESM (Cent.) as well as two extremes (H/W and C/D) whose role is to provide upper and lower bounds on the severity of future hypoxia.

In three future model runs, the forcings for the Reference simulation were adjusted to represent mid-21$^{st}$ century projected conditions (Table 1). These future forcings included atmospheric temperature, radiation (including net shortwave and downwelling longwave), wind speed and direction, terrestrial inputs (including freshwater and nutrient loads), conditions on the continental shelf (including water temperature and $O_2$), precipitation over the bay, and sea level. All future forcing fields were generated via the "delta method," as in Hinson et al. (2023). In this approach, ESM outputs were averaged over two thirty-year periods, one centered on 1995 (1981-2010) and the other on 2050 (2036-2065), and the differences between the two resultant past and future climatologies produced monthly climate deltas. These monthly deltas were interpolated to match the estuarine model grid and to provide daily atmospheric forcings. These were then added directly to the Reference atmospheric forcing fields to generate future atmospheric conditions, as well as to the atmospheric forcing fields for the CBP's Watershed Model. The resulting future watershed conditions (Hinson et al., 2023) only include modifications induced by atmospheric climate change, and do not include future changes due to human activity or nutrient management actions, which has been analyzed previously (Irby et al., 2018; Hinson et al., 2023) and is beyond the scope of this study.

Sea level, water temperature, and $O_2$ were adjusted on the continental shelf in the future model runs. Specifically, future changes to shelf water temperature and $O_2$ were derived from the non-downscaled oceanic components of the three selected ESMs. The oceanic outputs were first interpolated onto a common higher resolution grid (0.1°). Then for each ESM in the common

interpolated grid, results from the single grid cell closest to the estuarine model's land-sea boundary were used. Ocean water temperature from each ESM was averaged over the upper 40 meters of the ESM grids before calculating the monthly deltas or linearly interpolating to daily values. Each daily delta of depth-averaged ocean water temperature was added to all cells of the ROMS-ECB open boundary for all 20 vertical levels. Future oxygen at the boundary was computed assuming saturation using the future temperatures and the Reference salinity. Finally, the sea level change at the open boundary was derived using a quadratic model of relative sea level change from Boon and Mitchell (2018) fit to observational data from the NOAA tide station at Sewell's Point in Norfolk, VA. Boundary forcings for all other biogeochemical and physical variables were unchanged in the future runs.

Two suites of model runs were conducted. First, the Centroid, Hot/Wet, and Cool/Dry ESMs were each used in future model runs, using the forcings described above (Table 1). Secondly, climate variable runs were conducted to examine the relative roles of the various climate change factors, as projected by just the Centroid ESM. These model runs individually modified: air temperature (Tair), net shortwave and downwelling longwave radiation (Radiation), all watershed inputs (Watershed), sea level (SLR), wind speed and direction (Winds), continental shelf water temperature and $O_2$ (Shelf), and precipitation over the Bay (Precip). An additional two model runs were conducted to determine the relative impact of changes in shortwave (Swr) vs. longwave (Lwr) radiation.

# 3 RESULTS

## 3.1 ROMS-ECB evaluation

In the implementation described above, ROMS-ECB demonstrates reasonable skill in simulating key estuarine physical and biogeochemical variables (Table 2). When averaged across 25 CBP station locations (Fig. 1) and the full five years of the Reference simulation, modeled surface and bottom water temperature have only a small positive bias of 0.4 and 0.7 °C, respectively (Table 2). Salinity has a similarly small bias and is slightly underestimated at both surface and bottom. The model successfully captures the variability of both salinity and temperature, as shown by the similarity in standard deviation of the model results and observations and by their small root mean squared difference (RMSD; Table 2). Modeled $O_2$ is 0.4 mg $L^{-1}$ greater than observations at the surface and 0.1 mg $L^{-1}$ greater than observations at the bottom, which is similar to or less than biases reported in an earlier comparison of multiple Chesapeake Bay models (Irby et al., 2016). As with the physical variables, the standard deviations of modeled and observed $O_2$ are very similar, about ± 2 mg $L^{-1}$ at the surface and ± 3 mg $L^{-1}$ at the bottom (Table 2). Average modeled nitrate and DON also agree reasonably well with observations; however, modeled nitrate is overestimated, while modeled DON is underestimated, with both biases being greater at the bottom.

Model results for individual years also successfully reproduce the observed spatial patterns. For example, during the relatively low oxygen months of April to October, modeled salinity matches observations well, both at the bottom of the water column (Fig. 2a, c) and along the mainstem (Fig. 2b, d). During a year with lower-than-average freshwater flow, like 1992 (Fig. 2a, b), both modeled and observed salinity is higher by ~4.5 than during a higher-than-average flow year, like 1994 (Fig. 2c, d). ROMS-ECB also reproduces the upstream gradient of

high to low $O_2$ at the start of the Chesapeake Bay mainstem and Potomac tributary deep channels (Fig. 2e-h). The model performs similarly in years with higher freshwater flow ($RMSD_{1994}$ = 1.4 mg $O_2$ $L^{-1}$) compared to years with lower flow ($RMSD_{1992}$ = 1.5 mg $O_2$ $L^{-1}$) by matching the lower bottom $O_2$ concentrations observed farther south in the Bay during the higher runoff year (Fig. 2g, h). In the lower runoff year of 1992, both observed and modeled bottom $O_2$ are greater by an average of 0.28 mg $O_2$ $L^{-1}$ (Fig. 2e, f) compared to the higher runoff year of 1994. However, the model overestimates the southern mainstem bottom $O_2$ during 1992 and slightly underestimates the southern mainstem bottom $O_2$ during 1994.

Hypoxic volume computed from ROMS-ECB compares reasonably well with estimates calculated by interpolating observed $O_2$ profiles (Table 3, Fig. 3). For lower hypoxia thresholds, the agreement between the two models is higher, both in terms of percent and absolute values. From ROMS-ECB, AHV averaged over the 1991-1995 period is 4%, 20%, and 37% greater, for thresholds of < 1, 2, and 3 mg $O_2$ $L^{-1}$, respectively, than the analogous interpolated estimates (Table 3). The year-to-year variability in AHV for each $O_2$ threshold is greater in ROMS-ECB than in the interpolated estimates (Fig. 3). For example, ROMS-ECB shows substantially greater hypoxia than the interpolated estimates in the higher runoff years of 1993 and 1994, and slightly less hypoxia than the interpolated estimates within the other three years of the Reference simulation (1991, 1992 and 1995; Fig. 3). The seasonality of hypoxia in both models matches well, with hypoxia typically beginning in May, reaching the highest magnitude in July, and disappearing by October (Fig. 3). ROMS-ECB results tend to lead slightly ahead of the interpolated estimates in onset timing, whereas the timing of hypoxia dissipation is in reasonable agreement, given the large uncertainties associated with the interpolated estimates.

### 3.2 Mid-21st century hypoxia based on projections from three ESMs

Chesapeake Bay AHV increased between the Reference simulation and the three future ESM runs for almost all years examined (Fig. 4) and for both $O_2$ thresholds examined. The H/W run produced the greatest future increases in AHV, and the C/D run produced the smallest future increases (Fig. 4; Table 4). In the Centroid run, AHV ($O_2$ < 3 mg $L^{-1}$) increased by 23 ± 9 %, with the standard deviation representing the interannual variability among the five years of the model run. For the H/W and C/D runs, AHV ($O_2$ < 3 mg $L^{-1}$) increased by 36 ± 17% and 5 ± 8%, respectively (Fig. 4a; Table 4). The percent increases in AHV, for $O_2$ < 1 mg $L^{-1}$ in the three ESM runs, were more variable from year to year: Cent: 24 ± 16 %, C/D: -1 ± 14 %, H/W: 36 ± 28% (Fig. 4b; Table 4). The C/D run was the only ESM run that exhibited any decreases in AHV: Year 3 (an average temperature year with high runoff) showed a decrease of 28 $km^3$ d, for $O_2$ < 3 mg $L^{-1}$, and 75 $km^3$ d, for $O_2$ < 1 mg $L^{-1}$. However, the C/D run did not decrease in AHV every year: Year 1 (a lower runoff year with slightly higher temperatures) showed an increase of 352 $km^3$ d for $O_2$ < 3 mg $L^{-1}$ and 126 $km^3$ d for $O_2$ < 1 mg $L^{-1}$. For all three ESM runs, there was an expected pattern of larger absolute changes in hypoxic volume at the higher $O_2$ threshold ($O_2$ < 3 mg $L^{-1}$). The average difference in AHV between the H/W and C/D runs (471 $km^3$ d for $O_2$ < 3 mg $L^{-1}$ and 176 $km^3$ d for $O_2$ < 1 mg $L^{-1}$; Table 4) was less than the difference in AHV between a high runoff year (1994) and a low runoff year (1992) in the Reference simulation (1270 and 621 $km^3$ d; Table 3). The interannual variability also changed slightly between the Reference simulation and the future ESM runs. In the Centroid and H/W runs, the standard deviation increased for $O_2$ < 1 and 3 mg $L^{-1}$ by an average of ~29 $km^3$ d, which is respectively a ~10% and 5% increase in the 1991-1995 standard deviation. For the C/D run, the future standard deviation

decreased, from that of the Reference simulation, by ~9% and 4% respectively, for $O_2$ < 1 and 3 mg $L^{-1}$.

The seasonal start of hypoxia was projected to occur earlier in all three future ESM runs than in the Reference run, with the relative earliness of their hypoxia onsets being commiserate with their relative intensities of warming and runoff increase. The five-year averaged date at which bottom $O_2$ averaged over the mainstem dipped below 3 mg $L^{-1}$ occurred approximately two weeks earlier in 2046-2050 than in 1991-1995 (Fig. 5a). Only in the C/D run, in some lower runoff years, did the onset of hypoxia occur on the same day as in the Reference simulation (Fig. S1). In the H/W run, 2046-2050 hypoxia started earlier, relative to the 1991-1995 start dates, than had occurred in the Centroid or C/D runs (Fig. S1). Overall, the difference in hypoxia onset timing was slightly greater in years with average or lower freshwater than in years with higher discharge, like 1993 and 1994 (Fig. S1). Throughout the year, for the three ESM runs, bottom temperature was warmer (Fig. 5b). The warming in each ESM was commiserate with the earliness of their average hypoxia onset. The H/W run had an average spring-summer air temperature increase of 3.5 °C and had the earliest hypoxia start dates of the three ESM runs. Meanwhile, the C/D run had an average spring-summer air temperature increase of 1.5 °C and had the latest hypoxia start dates of the three ESM runs. Finally, the onset timing of hypoxia in the Centroid and H/W runs were more similar to each other than to the C/D run (Fig. S1). The Centroid and H/W runs were also more similar to each other with respect to their changes in freshwater discharge (72 and 74 $km^3$ $y^{-1}$, respectively) and DIN loading (116 and 119 Gg N $y^{-1}$, respectively). The C/D run had much lower freshwater discharge (63 $km^3$ $y^{-1}$) and DIN loading (100 Gg N $y^{-1}$) compared to the other two ESM runs (Table 1).

In the three future ESM runs, the spatial extent of hypoxic volume ($O_2$ < 3 mg $L^{-1}$) varied both with time and between model runs. Although hypoxic volume expanded vertically towards the surface in each run (Fig. 6a-c), the H/W run projected the greatest increases, and the C/D projected the smallest. Even more notably, the H/W and Centroid runs both expanded downstream in the mainstem (Fig. 6b, c), whereas the C/D run generated less hypoxia in the downstream direction than in the Reference simulation. For all future ESM runs, hypoxic volumes averaged over May-Oct experienced some mixture of expansion as well as recession downstream in the mainstem (Fig. 6d-f). For the Centroid and H/W runs, these recessions of hypoxic volume were south-east of the main body of hypoxia but do not appear in their respective transects. Of the three ESM runs, the C/D run produced the greatest recessions in hypoxic volume from 1991-1995 to 2046-2050. Averaging over the three future ESM runs, single month averages revealed seasonal variation in the hypoxic volume changes (Fig. 6g-l). The changes were greatest during May at the beginning of the hypoxic season (Fig. 6g, j). Then in July, mainstem hypoxia did not reach as far south (Fig. 6h, k). Finally, in September, near the end of the hypoxic season, there was once again some expansion of hypoxic volume in all directions (Fig. 6i, l).

### 3.3 Climate variable runs: relative roles of multiple climate change factors

The set of climate variable runs were conducted using deltas from the Centroid run to identify the climate change factors with the greatest impact on Chesapeake Bay hypoxia. On average, projected future increases in air temperature contributed the most to increases in modeled AHV (Fig. 7). In the $T_{air}$ run, AHV below thresholds of $O_2$ < 1, 2, and 3 mg $L^{-1}$ each respectively increased AHV by 18 ± 6%, 17 ± 5%, and 17 ± 3%, with the standard deviations representing interannual variability (Table 4). The next largest increase in average AHV, for

most $O_2$ concentrations, occurred in the Watershed run. The $T_{air}$ run also contributed the most to the early onset of hypoxia compared to the other climate variable runs (Fig. 5).

Future changes in less well-studied climate variables such as winds, non-runoff precipitation, radiation, and ocean water conditions had small impacts on projected mid-21$^{st}$ century Chesapeake Bay hypoxia, compared to the influences of future warming, sea level, and terrestrial runoff (Table 4; Fig. 7). The five-year average increase in AHV from changing winds, non-runoff precipitation, radiation, and ocean water conditions were each less than 4%, and substantially less than the differences in impact between the various climate model runs (~15-18%). The next largest changes in future AHV were due to future changes in radiation and then shelf conditions. For all $O_2$ thresholds, five-year averaged change to AHV was very small in the Winds and Precip runs. For lower $O_2$ thresholds, the SLR run produced large decreases in AHV compared to the Reference, but for $O_2 < 3$ mg $L^{-1}$, AHV increased slightly.

**3.4 Climate variable runs: interannual variability**

From year to year, some climate variable runs had different impacts on AHV, either increasing or decreasing. In the $T_{air}$ run, there was some small interannual variation, with the greater increases in HV occurring in the two higher runoff years (Years 3 and 4, Fig. 8; Table S1). Regardless of specific year, the Radiation run followed the same year-to-year pattern as SLR, in terms of positive or negative impact on AHV, but Radiation caused smaller magnitudes of change. Meanwhile, the Watershed and SLR runs had opposing impacts on AHV. The sign, positive or negative, of the change in AHV from these two runs varied with the freshwater discharge of each year (Fig. 8; Table S1). In lower runoff years like 1991, 1992 and 1995, the Watershed run produced increases in AHV while in higher runoff years like 1993 and 1994 the Watershed run decreased AHV. Except for the Watershed run, all climate variable runs showed

the largest absolute magnitude of change in AHV during the high runoff year 1994. Lastly, the Winds run showed changes in AHV during the years 1994 (-39 $km^3$ d) and 1995 (34 $km^3$ d), that were closer in magnitude to the average change from the Watershed run (69 $km^3$ d).

Within any given year, the impacts of some climate variable runs on daily hypoxic volume are more important than their impacts on AHV. For most years and climate variable runs, the greatest increases in HV occurred between April and June. The average impact on hypoxia of the Radiation run appeared small when examining just AHV; however, this was due to the interannual variability and seasonality (Fig. 8). Throughout all five years of the Radiation run, HV increased in the spring and early summer and then HV decreased for most of the remaining hypoxic season. The two additional climate variable runs, Swr and Lwr, behaved additively when summed and compared with the Radiation run (Fig. S2). The seasonality of changes in the Radiation run was the same as in the Swr run, with a small shift that had little seasonal variability from the Lwr run. Due to this additive relationship, only results from the Radiation run are shown. Changes to HV were again small in the future Shelf and Precip runs (Fig. 8). Changes to HV in the future Winds run, during the two years in which it had larger AHV, were small in magnitude but persistent through time.

### 3.5 Changes in modeled $O_2$ solubility, production and consumption

From the Reference simulation to the mid-21$^{st}$ century of the $T_{air}$ and Centroid runs, reduced $O_2$ solubility appeared to exert more influence, than the changes to biogeochemical processes, on future hypoxia in the spring (Fig. 9). Primary production dominated as a source of $O_2$ in the surface waters (upper ~5m), while biogeochemical sinks of $O_2$ dominated below surface layers (Fig. 10a-f). The sinks include aerobic remineralization processes both within the water column and at the water/sediment interface and are, from here on, collectively referred to

here as respiration. Starting in May, the scarcity of $O_2$ became limiting to respiration in the water column. In the $T_{air}$ run, $O_2$ became limiting earlier by about 2 weeks and, through the summer, continued to be more limiting than in the Reference (Fig. 9a). Respiration became limited earlier, because $O_2$ reached lower values quicker (Fig 5a, c). One mechanism that accounted for the earlier decrease in $O_2$ was the change in solubility of $O_2$. During an average year, reduced solubility could have accounted for the majority of the changes in bottom $O_2$ (Fig. 9b). The actual change in $O_2$, from 1991-1995 to 2046-2050, eventually became less than the change in solubility; which indicated that, in late spring and summer, changes to respiration were more impactful to change in $O_2$ and by extension hypoxia.

Respiration and production in the future climate variable runs both increased and decreased depending on the time of year and location in the Bay (Fig. 10). Respiration in the $T_{air}$ run slightly increased early in the year (Fig. 10g). This early increase in respiration slightly decreased $O_2$, in addition to the effect of reduced solubility, which contributed to $O_2$ becoming more limiting in spring (Fig. 9). After March, respiration was decreased throughout spring and early summer (Fig. 10i, k). Production in the $T_{air}$ run mostly increased throughout the entire year, and respiration, outside of summer, mostly increased throughout the water column and year as well (Fig. 10g-l). Despite the decrease in respiration that occurred in the deeper parts of the water column, hypoxia still expanded during those times. This occurred because respiration was decreasing in those locations where hypoxia was already experienced in 1991-1995, but respiration increased just outside of this historically hypoxic volume. In the Radiation run, the changes in production and respiration were less variable through time and space than in the $T_{air}$ run. Increased future radiation increased production and respiration throughout the year and most of the mainstem. Before April in the Watershed run, respiration and production were mostly

decreased in the mainstem, but after April, respiration and production increased (Fig. 10s-x). In the SLR run, in an average year, production increased upstream, in shallower depths, and decreased downstream. Respiration increased in areas immediately beneath the increases in production (Fig. 10y-D). In the Centroid run, the changes in production and respiration reflected the changes in the climate variable runs, with the impacts of the $T_{air}$ and Watershed run dominating.

# 4 DISCUSSION

## 4.1 Relative roles of atmospheric, terrestrial, and oceanic forcings

Of the various atmospheric, terrestrial, and oceanic changes exhibited by the mid-21$^{st}$ century, warming will likely have the greatest influence on future hypoxia in the Chesapeake Bay primarily due to a reduction in solubility as well as to an increase in the rates of respiration and remineralization. The impact of temperature on stratification, on the other hand, is expected to be minor in comparison as Hinson et al. (2022) has shown that temperature will likely warm throughout the water column in the relatively shallow Chesapeake Bay. Specifically, our study showed that projected warming decreases the concentration of $O_2$ saturation in bottom waters by ~0.4-0.5 mg $O_2$ $L^{-1}$ (Fig. 5c) during winter and spring, which is consistent with previous studies (Irby et al., 2018; Tian et al., 2022). Summer decreases in oxygen are typically lower, since in much of the deepest regions of the Bay $O_2$ concentrations are already lower than saturation, so they cannot undergo as large reductions. As a result, hypoxia starts earlier in the year, and this earlier onset of hypoxia accounts for a sizable portion of the total hypoxic volume increase due to warming. Warming additionally increases both production and respiration across the Bay, however, since respiration dominates in the dark bottom waters and typically increases with

temperature faster than production, these changes have the potential to further reduce bottom $O_2$ concentrations in early spring (Fig 10g). However, during late spring through summer, $O_2$ uptake due to respiration is actually decreased where hypoxia is already occurring, due to greater $O_2$ limitation (Fig. 9a) and a reduction in the availability of organic matter, which has been respired earlier in the season. At the same time, respiration is still increasing where hypoxia had not previously been (Fig. 10i), hence its expansion. The increases in respiration higher in the water column and reduction of bottom and lower water column respiration are consistent with results reported by a previous Chesapeake Bay modeling study (Ni and Li, 2023). They found that sediment oxygen demand was reduced and water column respiration increased.

Projected watershed runoff changes increase Chesapeake Bay hypoxic volumes on average, but also demonstrate important seasonally and spatially explicit decreases in hypoxic volumes. As seen in prior studies, such as Frankel et al. (2022), the southern extent of hypoxia is sensitive to changes in forcing conditions like nutrient loading. In our study, the largest mainstem volumes of water that became hypoxic, under future watershed conditions, are downstream from and vertically above the hypoxic volumes in the Reference simulation (Fig. 10u). This spatial dynamic of increasing hypoxia is, in part, due to changes in nutrient availability. Projected future inorganic nitrogen loading increases during the large increases in freshwater discharge, though inorganic nitrogen concentrations of watershed runoff decrease due to warming and enhanced potential evapotranspiration over the watershed (Bhatt et al., 2023). However, bottom $O_2$ in the deep mainstem channel increases during February to April (Figure 5g). While the increase in the dissolved inorganic nitrogen loading is generally consistent with prior work (Bhatt et al., 2023; Hinson et al., 2023), the average seasonal changes, outside of summer, in Chesapeake Bay $O_2$ were not previously reported. The increase in bottom $O_2$, from

winter to early spring, is caused by decreases in respiration (Fig. 10s) due to reduced concentrations of phytoplankton, semilabile dissolved organic nitrogen, and detrital nitrogen in the deep mainstem. The decreases in organic nitrogen and respiration result from the strong increases in respiration upstream of the deep channel, and upstream respiration increases due to increased water temperature from the watershed. Downstream respiration increases mid-way through April, bringing bottom $O_2$ lower than in 1991-1995; because, freshwater discharge greatly increases during April and transport of dissolved inorganic nitrogen downstream also increases such that phytoplankton, semilabile DON, and detrital nitrogen increase downstream. This summer-time decrease in bottom $O_2$ and increase in hypoxia is consistent with the results reported by other studies that examined the impact of having greater watershed loading (Ni et al., 2020; Frankel et al., 2022; Hinson et al., 2023).

The impact of future sea level rise on hypoxia is complex, and depends on the threshold of $O_2$ used to define hypoxia. Specifically, reductions in hypoxic volume occur where $O_2 < 1$ and 2 mg $O_2$ $L^{-1}$, while increases in hypoxia occur for slightly higher concentrations: 2 mg $L^{-1} < O_2 <$ 3 mg $L^{-1}$ (Fig. 7). The increases in bottom oxygen concentration are due to Bay water temperatures being cooler during spring and summer. As described by St-Laurent et al. (2019), in the future when sea level rise has caused the volume of Bay water to be greater, the Bay will take longer to warm up each spring and longer to cool off each fall. This results in cooler temperatures and higher oxygen concentrations in early summer, and warmer temperatures and lower oxygen concentrations each fall. Prior Chesapeake Bay sea level rise modeling studies attributed their reported increases in bottom $O_2$ to enhanced gravitational circulation (Wang et al., 2017; Cai et al., 2022). Cai et al. (2022) describes the impact on bottom $O_2$ of enhanced circulation as being minor compared to other effects of sea level rise. The more impactful effects

of sea level rise documented by Cai et al. (2022) included an upward shift in pycnocline height as well as enhanced rates of production and respiration. In this work, the pycnocline height and salinity gradient increased from much of the upper mainstem, though less so in the deeper mainstem. Cai et al. (2022) also found production increased in shallower portions of the Bay, due to increased light availability from a deepening of the euphotic zone in the shallow areas, where the mixed layer depth is deeper than the euphotic zone depth. Increases in production and phytoplankton concentration, in the shallower portions of the Bay, occur here as well. The increase in production, in shallow regions, is followed by increased respiration lower in the water column of those shallow areas (Fig. 10y-D). From these effects on Bay stratification and biology, Cai et al. (2022) found that hypoxia, for $O_2 < 2$ mg $L^{-1}$, increased under sea level rise. Because this work reports changes in multiple $O_2$ thresholds for hypoxia, a more nuanced combination of decreases as well as increases are found. Respiration decreases in the deep mainstem, where 1991-1995 $O_2$ reaches < 1 and 2 mg $L^{-1}$, and respiration increases in shallower portions of the mainstem, where 1991-1995 $O_2$ was on average above 2 mg $L^{-1}$, so hypoxic volume grows for higher $O_2$ thresholds and shrinks for lower thresholds.

Somewhat surprisingly, projected increases in future radiation increase hypoxia in the spring, but decrease hypoxia in the summer, which may mask the importance of future radiation when only looking at annual estimates of hypoxia. In fact, in spring (April to May) the increase in hypoxia due to future increases in radiation is similar in magnitude to the increase in hypoxia due to changes in watershed inputs. Early spring increases in radiation fuels more production at the surface through increased light and water temperature, which ultimately increases remineralization at depth as more organic matter sinks. Then as summer progresses, since inorganic nutrients and organic matter are used up earlier, there is less $O_2$ consumption and less

hypoxia later in the summer. By July, the reductions in hypoxia due to radiation changes are nearly equal in magnitude to the spring increases in hypoxia. This shift in the timing of hypoxia is due specifically to the increase in future *shortwave* radiation, which raises water temperature and increases light availability for phytoplankton growth. In contrast, future *longwave* radiation only increases water temperature which results in reduced $O_2$ throughout the year, with no impact on the phenology of future hypoxia. These results have not been noted in prior studies investigating future changes in Chesapeake Bay hypoxia, as changes in shortwave and longwave radiation have not previously been considered in isolation. There are some prior cases, outside of the Chesapeake Bay, of coastal hypoxia studies including future projections of shortwave and longwave radiation (Hafeez et al., 2021; Huggett et al., 2021; Duvall et al., 2022); however, they do not isolate the impact of changes to these variables.

Changes in winds and direct precipitation onto the Bay surface had only a minor influence on future changes in hypoxia. Although wind speed and direction are important factors in governing hypoxia in the Chesapeake Bay (Scully, 2010, 2016a, b), as well as in other regions such as the Pearl River Estuary (Hong et al., 2022) and Cape Cod Bay (Scully et al., 2022), future wind changes are shown to be small in our region (Table 1). As a result, this studies indicates that they will likely have only a minor influence on future hypoxia. Direct precipitation onto the Bay surface similarly had only a minor impact on hypoxia. This is due not only to the relatively small annual change projected for precipitation over the Bay (Table 1), but also because the dominant source of freshwater to the Bay comes from terrestrial runoff rather than direct precipitation. However, the change in winds and non-runoff precipitation in our analysis may be artificially dampened by our use of the delta method (Bhatt et al., 2023; Hinson et al., 2023; Linker et al., 2024). For variables like wind speed and direction, in which the daily,

seasonal, and annual variation is important to the timing and intensity of hypoxia, our addition of monthly deltas to the 1991-1995 reference forcings may not have properly accounted for potential changes in daily or interannual patterns in wind and precipitation. The use of monthly deltas may shift the phenology of winds, but the magnitude of those monthly changes are still smoothed out to smaller values by the 30-year monthly averaging of downscaled earth system model outputs. Following a study from Hinson et al. (2023), it may be more likely that directly using earth system model outputs as the estuarine model forcings over a long continuous model run of 1991-2050 would yield greater changes in hypoxia due to winds or even non-runoff precipitation.

At the other end of the Bay, future temperature and $O_2$ concentrations in the coastal ocean have a relatively small impact on hypoxia within the Bay. This is primarily because the changes in these fields mostly impact the estuary south of where hypoxia typically forms. While future ocean temperatures are projected to increase by roughly the same amount as atmospheric temperatures (Table 1), oceanic temperatures impact Bay temperature only in the southern portions of the mainstem. This is consistent with the results of Hinson et al. (2022), who showed that, over the past 35 years, warmer ocean waters have been primarily influencing only the southern mainstem Bay where nutrients are limiting enough to prevent excess production and hypoxia formation.

### 4.2 Interannual variability

In modeling hypoxia in estuarine systems, natural variation in surrounding conditions can introduce large uncertainties (Meier et al., 2021). For the early 1990s, there is a large amount of variability in the duration and extent of hypoxia from one year to the next. The pattern of interannual variation in hypoxia is set in the 1991-1995 Reference simulation, in which hypoxia

is greatest during years with higher than average freshwater discharge and smallest in years with lower than average discharge. This year-to-year pattern of higher runoff resulting in greater volumes of hypoxia is not changed in any future run. That is to say that, while the future impacts of climate change on hypoxia are important to consider, climate change will not alter hypoxia to such an extent that interannual variability would become of secondary importance. However, under future conditions, the change in hypoxia from 1991-1995 to 2046-2050 does not always have the same pattern as that of the absolute hypoxia. The control of freshwater discharge and nutrient loading on the hypoxia in the Chesapeake Bay is generally well understood (Wang et al., 2015). However, less well studied is how projected future changes in hypoxia vary by year, based on underlying hydrographic conditions.

With all climate changes from the Centroid earth system model, the percent change in annual hypoxic volume was greater during years with lower than average freshwater discharge and lower during high discharge year (Table S2). This difference in impact is due to the future changes over the watershed. Like in the future predicted by the Centroid earth system model, under just those future climate changes to the watershed, hypoxia increases in low runoff years but decreases in high runoff years. This year-to-year change in climate impact is a result of how freshwater discharge and dissolved inorganic nitrogen loading change in each year. The strong decrease in freshwater input and dissolved inorganic nitrogen loading during April of those two high runoff years reduces respiration throughout the Bay, though production and respiration still locally increase in a small upstream range because of the warmer freshwater inputs. Lower percent increases in hypoxia during high runoff years is also found in the results of a present day scenario without nutrient reductions (Frankel et al., 2022). In their model experiments, they had separated the impacts on hypoxia of changes to watershed temperature and loading. Frankel et al.

(2022) reported that in years with higher runoff, hypoxia decreased by greater volumes than in years with lower runoff. From both this study and Frankel et al. (2022), it is clear that changes in loading and freshwater discharge cause the majority of watershed induced changes to Chesapeake Bay hypoxia, and changes in watershed temperature have contributing but minor effects.

In two of the future climate variable runs, sea level rise and increased radiation, there were changes to hypoxic volume that were the inverse of the interannual pattern produced by future climate change over the watershed. During lower runoff years, sea level rise and future increased radiation produced less hypoxic volume for all $O_2$ thresholds; however, in high runoff years, they increased hypoxia. In both runs, their impacts on production and respiration are similar such that they share this pattern in future hypoxia changes. With future sea level rise, the boosts in production occur in the light-limited, shallow upstream portion of the mainstem. Subsequently respiration increases in that same portion of the Bay. During lower runoff years, the inorganic nitrogen loading is low enough such that the increased upstream production and respiration depletes the inorganic nutrients before reaching farther downstream. Then, during higher runoff years, there is enough loading that nutrients are able to reach farther downstream to fuel more production and subsequent respiration. Given that spring-summer temperature decreases with sea level rise and increases with future increased radiation, it is not surprising that, during low runoff years, sea level rise decreases annual hypoxic volume ($O_2 < 3$ mg $L^{-1}$) more than increased radiation. Conversely, during high runoff years, sea level rise produces larger hypoxic volume increases than future radiation. Unfortunately, there has not previously been any prior studies that have compared the individual impacts of increased shortwave and longwave radiation to that of sea level rise on coastal hypoxia.

### 4.3 Sensitivity to Earth System Model

By using projections from multiple future climate models, the estuarine model's high sensitivity to changes in input variables, especially air temperature, fresh water discharge, and inorganic nitrogen loading, is accounted for. Past coastal modeling studies have focused on the analysis of sources of uncertainty in studying estuarine biogeochemistry and the impacts of climate change (Meier et al., 2019, 2021; Hinson et al., 2023). While sources of uncertainty were not a primary focus, this study follows the advice of past works by using an ensemble of earth system model climate projections, over all possible model boundaries. The three earth system models produced quite different predictions of hypoxia (Fig. 4). The differences in hypoxia between the three model runs was mostly due to the differences in earth system model predictions of warming, freshwater discharge, and inorganic nitrogen loading (Table 1). Differences in freshwater discharge and nutrient loading between earth system models appears to have equal impact on AHV as differences in warming between earth system models. From the Cool/Dry to Centroid runs, the difference in both absolute and percent change in AHV is approximately double the difference in percent change from the Centroid to the Hot/Wet runs. The average change in warming in each earth system model is about evenly spaced, with the Hot/Wet and Cool/Dry being approximately 1°C higher and lower, respectively, than the Centroid. However, the future change in discharge and loading in the Centroid and Hot/Wet runs are quite similar in magnitude, phenology, and interannual variation. Meanwhile, the Cool/Dry run has distinctly lower future discharge and loading, throughout most of 2046-2050, than both the Centroid and Hot/Wet runs. The Cool/Dry has similar phenology but lower magnitude in discharge and loading changes during the two higher reference runoff years. During lower reference runoff years, Cool/Dry produced inverted, with respect to sign, discharge and loading

changes as the Centroid and Hot/Wet runs. The importance of considering variation in earth system model projections over the watershed can not be understated. Many prior studies have focused on assessing the large impacts of atmospheric climate change (Wang et al., 2017; Meier et al., 2021; Tian et al., 2022). While these impacts are large, this study and others have shown that climatological changes to freshwater discharge and nutrient loading are also key (Ni et al., 2020; Hinson, 2023; Hinson et al., 2023).

# 5 CONCLUSIONS AND MANAGEMENT IMPLICATIONS

The future projections analyzed in this study included changes to air temperature, radiation (shortwave and longwave), winds (magnitude and direction), non-runoff precipitation directly onto the Bay surface, ocean shelf conditions (both temperature and oxygen), watershed inputs (both nutrient loading and freshwater discharge), and sea level rise. The results reported here demonstrate that future changes in radiation, winds, non-runoff precipitation, and shelf conditions are each likely to cause only small changes (< 1%) in future AHV. As has been seen in prior studies (Irby et al., 2018; Ni et al., 2019), future warming, watershed nutrient loading changes, and sea level rise will likely account for the greatest impacts on future Chesapeake Bay hypoxia; thus managers should continue to prioritize the future climate impacts of warming, changing terrestrial runoff and sea level rise.

While future changes in radiation, winds, non-runoff precipitation, and shelf conditions are not very impactful on hypoxic volume when integrated over the hypoxic season, they do present some questions for future study. The magnitude of projected changes in daily hypoxic volume due to future shortwave and longwave radiation may still be important for managers to consider given that the set water quality standards are not evaluated by AHV, but by $O_2$. Future

changes in winds may still be more impactful than is shown here, but the delta method applied in this study may underestimate the changes in wind. Following Hinson et al. (2024), performing future climate projection experiments, either as continuous runs or discrete reference and time frames, while using downscaled climate model outputs directly as the estuarine model forcings, instead of calculating and adding deltas onto past forcings not from the climate models, should be a direction for future study.

This study also demonstrates that compared to conditions in the early 1990s, hypoxia may start two weeks earlier on average by the mid-21$^{st}$ century, but become less pronounced by mid-summer. The large spring increases are due to lowered initial $O_2$ from reduced solubility. Late spring and summer increases in hypoxic volume are due to increased respiration in the water column, while reduction in hypoxic volume in the summer is due to respiration becoming limited by $O_2$ and organic nitrogen. A potential future, in which hypoxia is more seasonally and interannually variable, presents a more serious risk to the stability of future fisheries and aquaculture. Modeling of $O_2$ dynamics alone may not be able to capture the full extent of impacts on fish habitat. Future work building from this and related studies should seek to incorporate the impacts on fisheries.

Our work provides mid-21$^{st}$ century estimates of hypoxic conditions in Chesapeake Bay, based on downscaled projections from three climate models, including two extremes (i.e., relatively hot and wet vs. cold and dry models) as well as a model that projects more typical future conditions. The more typical climate model resulted in increases of 13% up to 35% in Chesapeake Bay AHV since 1991-1995 (when defined as $O_2 < 3$ mg $L^{-1}$), with higher runoff years resulting in smaller percent hypoxia increases. Averaged over the five years examined, the warmer and higher runoff mid-21$^{st}$ century climate projection resulted in a 36% average increase

in Chesapeake Bay AHV, while the cooler and lower runoff projection resulted in only a 5% average increase, compared to the centroid model projection of a 21% increase. In line with prior studies (Hinson et al., 2023; Ni et al., 2019), the results of this study continue to point towards the practice of an ensemble approach when applying climate change projections, using output from multiple regionally downscaled climate models. Given the high variability in future hypoxic volume predictions, due to both interannual variation as well as choice of climate model, it is important that Chesapeake Bay managers consider both sources of variability.

# TABLES

**Table 1.** Estuarine model forcing (averages and standard deviations) and the three sets of future ESM deltas averaged over time (daily) and space for the Reference simulation.

| Boundary | Forcing Variable | 1991-1995 | 2046-2050 Centroid Delta | 2046-2050 Cool/Dry Delta | 2046-2050 Hot/Wet Delta |
|---|---|---|---|---|---|
| Atmosphere | Air Temperature (°C) | 14.6 | 2.3 | 1.2 | 3.3 |
| | Net Shortwave Radiation (W $m^{-2}$) | 160 | 8.4 | -0.04 | 11 |
| | Downwelling Longwave Radiation (W $m^{-2}$) | 327 | 10 | 7.1 | 14 |
| | Wind Speed (m $s^{-1}$) | 4.2 | 0.01 | 0.04 | 0.04 |
| | Wind Direction (deg) | 4.6 | 0.4 | 0.4 | 0.8 |
| | Precipitation (mm $d^{-1}$) | 3.1 | 0.14 | 0.03 | 0.19 |
| Watershed | Freshwater Mass Transport ($km^3$ $y^{-1}$) | 68 | 3.8 | -4.9 | 5.7 |
| | DIN Loading (Gg N $y^{-1}$) | 108 | 7.7 | -7.4 | 11 |
| | Terrestrial Water Temp. (°C) | 15.9 | 0.6 | 0.2 | 0.9 |
| Ocean | Sea Level (m) | -0.13 | 0.48 | 0.48 | 0.48 |
| | Ocean Water Temp. (°C) | 13.5 | 2.5 | 0.6 | 3.6 |
| | Ocean Oxygen (mg $O_2$ $L^{-1}$) | 8.6 | -0.4 | -0.1 | -0.5 |

*Wind Direction is given as degrees North of East and by oceanographic convention (toward its direction, not from)

**Table 2.** Comparison of results from the Reference simulation and observations; mean ± standard deviation, mean bias, and mean root mean squared difference (RMSD) were calculated over 25 stations (Figure 1).

| Variable | Depth | 1991-1995 (Reference) | Observed | Mean Bias | Mean RMSD | N* |
|---|---|---|---|---|---|---|
| Temperature ($^oC$) | Surface | 17.6 ± 8.0 | 17.2 ± 8.2 | 0.4 | 0.9 | 1953 |
| | Bottom | 17.0 ± 7.3 | 16.3 ± 7.5 | 0.7 | 1.4 | 2265 |
| Salinity | Surface | 13.0 ± 6.4 | 13.6 ± 6.5 | -0.6 | 1.8 | 1931 |
| | Bottom | 18.7 ± 6.8 | 19.4 ± 6.5 | -0.7 | 2.2 | 2265 |
| $O_2$ (mg $O_2$ $L^{-1}$) | Surface | 9.6 ± 2.0 | 9.2 ± 2.0 | 0.4 | 1.3 | 1928 |
| | Bottom | 5.6 ± 3.0 | 5.5 ± 3.4 | 0.1 | 1.6 | 2076 |
| $NO_3^-$ (mmol N $m^{-3}$) | Surface | 23.6 ± 35.4 | 18.7 ± 26.9 | 4.9 | 18.6 | 1719 |
| | Bottom | 17.4 ± 24.0 | 9.4 ± 17.3 | 8.0 | 13.6 | 1470 |
| DON (mmol N $m^{-3}$) | Surface | 20.6 ± 11.0 | 21.7 ± 6.9 | -1.1 | 13.4 | 1861 |
| | Bottom | 18.2 ± 7.0 | 21.1 ± 6.7 | -2.9 | 9.6 | 1458 |

*Number of data points included in the comparisons.

**Table 3.** Comparison of modeled AHV with AHV estimates calculated by interpolating observed oxygen concentrations. Averages ± standard deviations were calculated over the period of the Reference run (1991-1995).

| $O_2$ Threshold | ROMS-ECB AHV ($km^3$ d) | Interpolated AHV ($km^3$ d) |
|---|---|---|
| $O_2 < 3$ mg $L^{-1}$ | 1519 ± 613 | 1111 ± 157 |
| $O_2 < 2$ mg $L^{-1}$ | 916 ± 458 | 761 ± 163 |
| $O_2 < 1$ mg $L^{-1}$ | 488 ± 305 | 467 ± 146 |

**Table 4.** Five-year averaged AHV for the three future ESM runs, Centroid, Hot/Wet (H/W) and Cool/Dry (C/D) and increases in AHV between 1991-1995 (listed in Table 3) and the climate variable runs.

| Model Runs | 2046-2050 AHV ($km^3$ d) | | Increase in AHV ($km^3$ d) (2046-2050 minus 1991-1995) | |
|---|---|---|---|---|
| | < 1 mg $O_2$ $L^{-1}$ | < 3 mg $O_2$ $L^{-1}$ | < 1 mg $O_2$ $L^{-1}$ | < 3 mg $O_2$ $L^{-1}$ |
| Centroid | 605 ± 327 | 1874 ± 656 | 117 ± 57 | 355 ± 92 |
| C/D | 485 ± 273 | 1587 ± 597 | -3 ± 51 | 69 ± 88 |
| H/W | 661 ± 327 | 2058 ± 639 | 174 ± 33 | 539 ± 60 |
| $T_{air}$ | 574 ± 341 | 1769 ± 670 | 86 ± 38 | 251 ± 61 |
| Watershed | 521 ± 270 | 1588 ± 520 | 33 ± 43 | 69 ± 97 |
| SLR | 468 ± 321 | 1525 ± 699 | -20 ± 26 | 6 ± 93 |
| Radiation | 496 ± 318 | 1528 ± 634 | 8 ± 17 | 9 ± 32 |
| Shelf | 495 ± 308 | 1527 ± 610 | 7 ± 5 | 8 ± 9 |
| Winds | 490 ± 297 | 1521 ± 596 | 2 ± 13 | 2 ± 27 |
| Precip | 486 ± 303 | 1517 ± 610 | -1 ± 4 | -2 ± 6 |

FIGURES

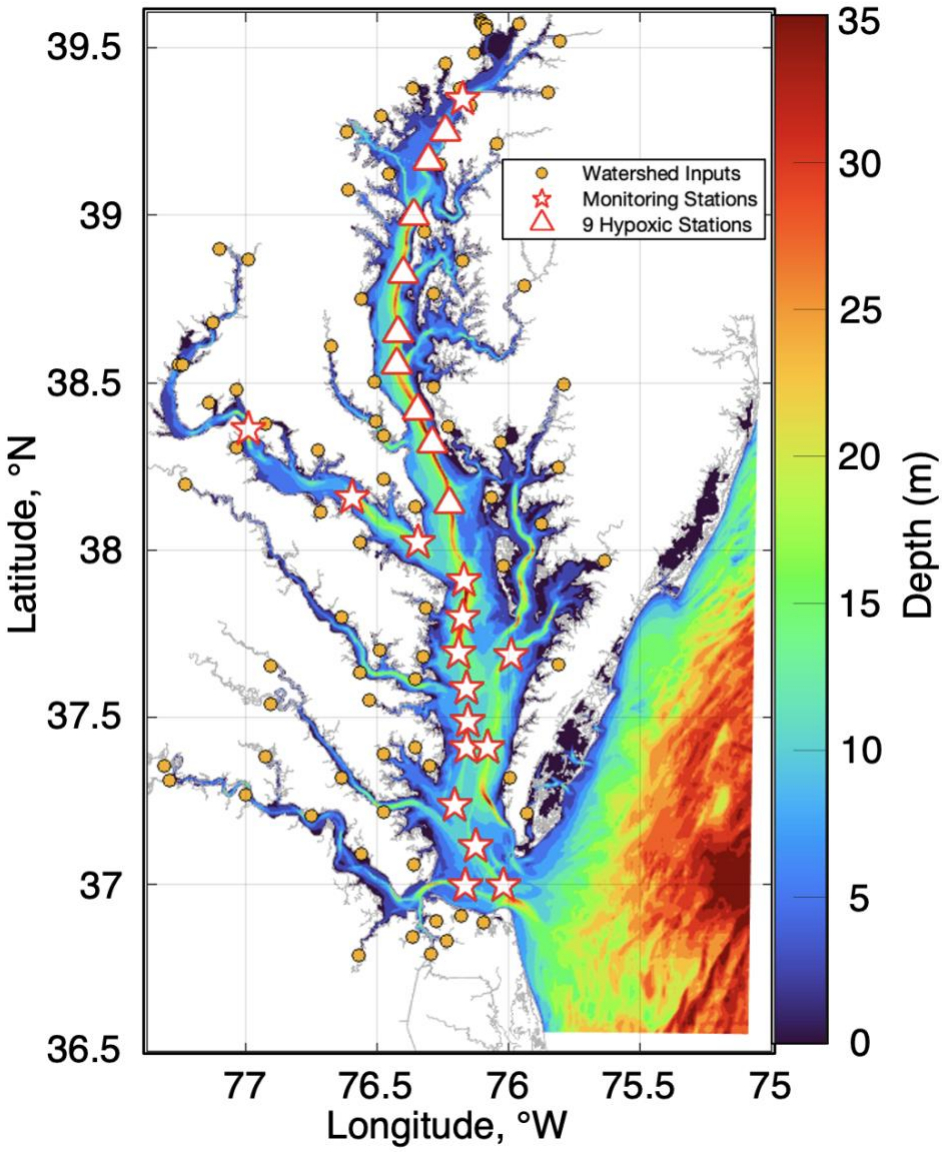


**Figure 1.** Model bathymetry, watershed input locations, and CBP water quality monitoring stations used for model evaluation, including those where modeled hypoxia consistently occurs in the Reference simulation.

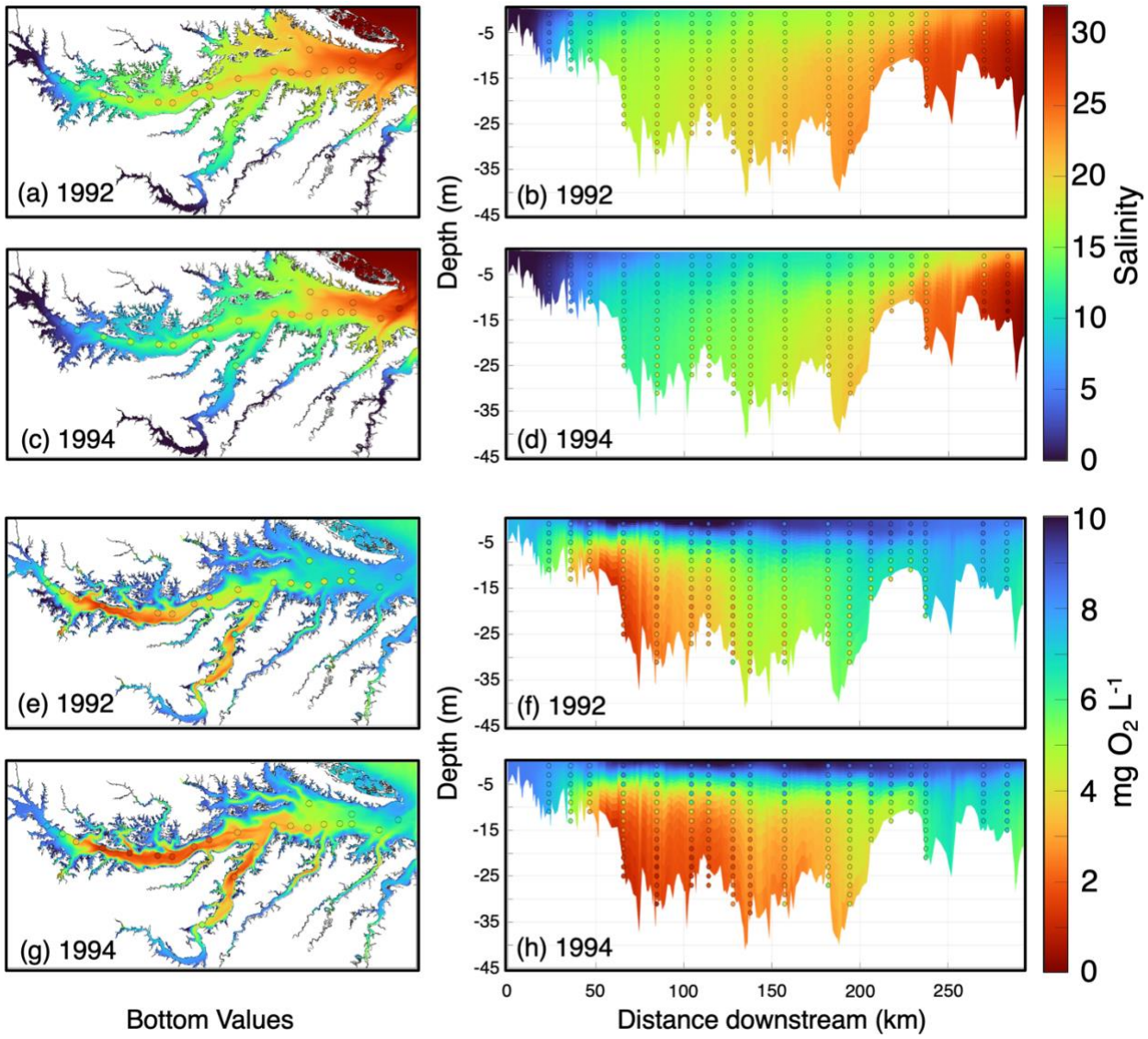


**Figure 2.** Modeled bottom salinity (a-d) and bottom oxygen (e-h) averaged from April to October for a low-runoff year (1992; a-b, e-f) and a high-runoff year (1994; c-d, g-h). Transects are plotted along the deepest part of the mainstem. Observed values are superimposed as colored circles.

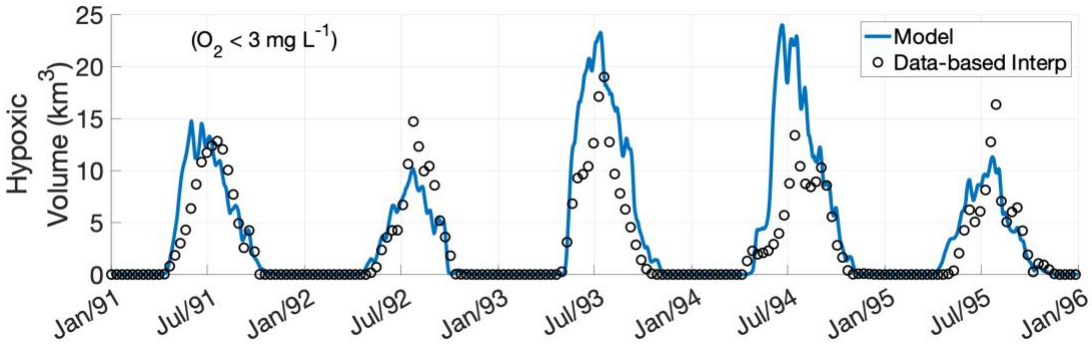


**Figure 3.** Hypoxic volume computed from the ROMS-ECB Reference run and interpolated $O_2$ profiles (Bever et al., 2018) using the threshold of $O_2 < 3$ mg $L^{-1}$.

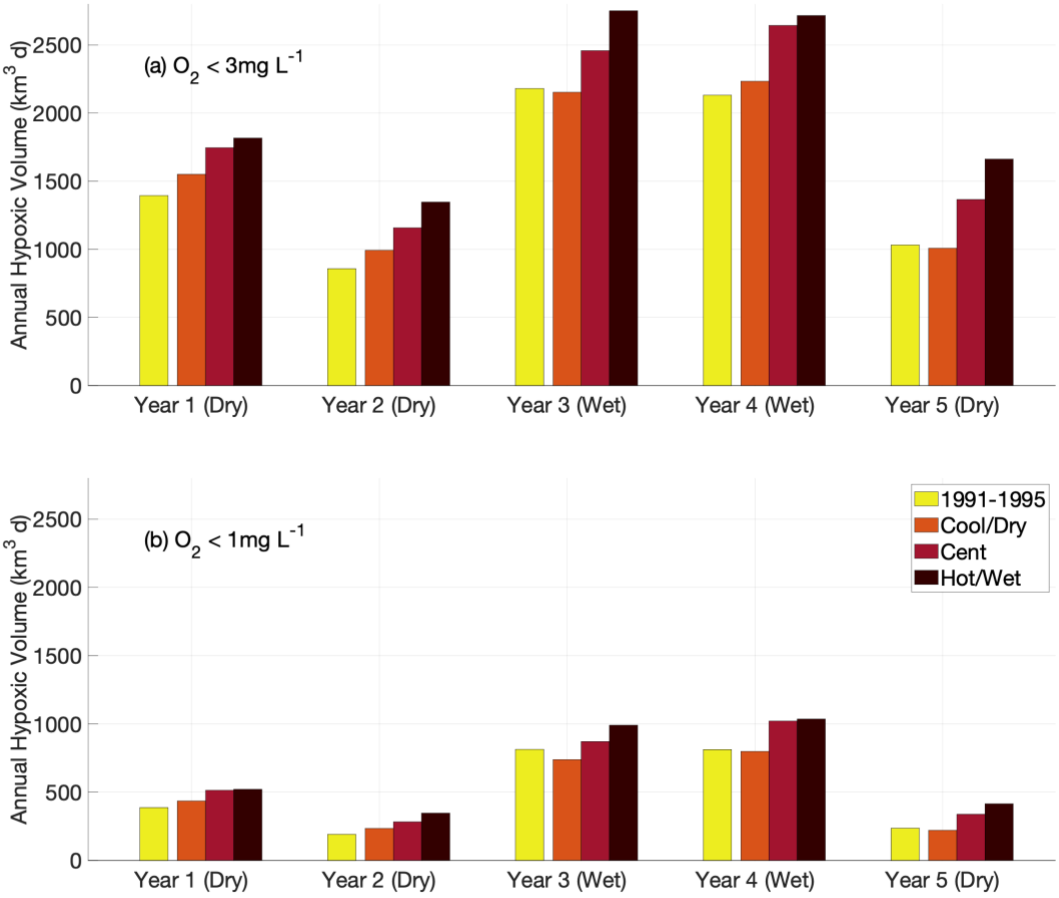


**Figure 4.** Annual Hypoxic Volume (AHV) from the Reference simulation and the three future ESM runs, for all five years of each model run, as defined by (a) $O_2 < 3$ mg $L^{-1}$ and (b) $O_2 < 1$ mg $L^{-1}$.

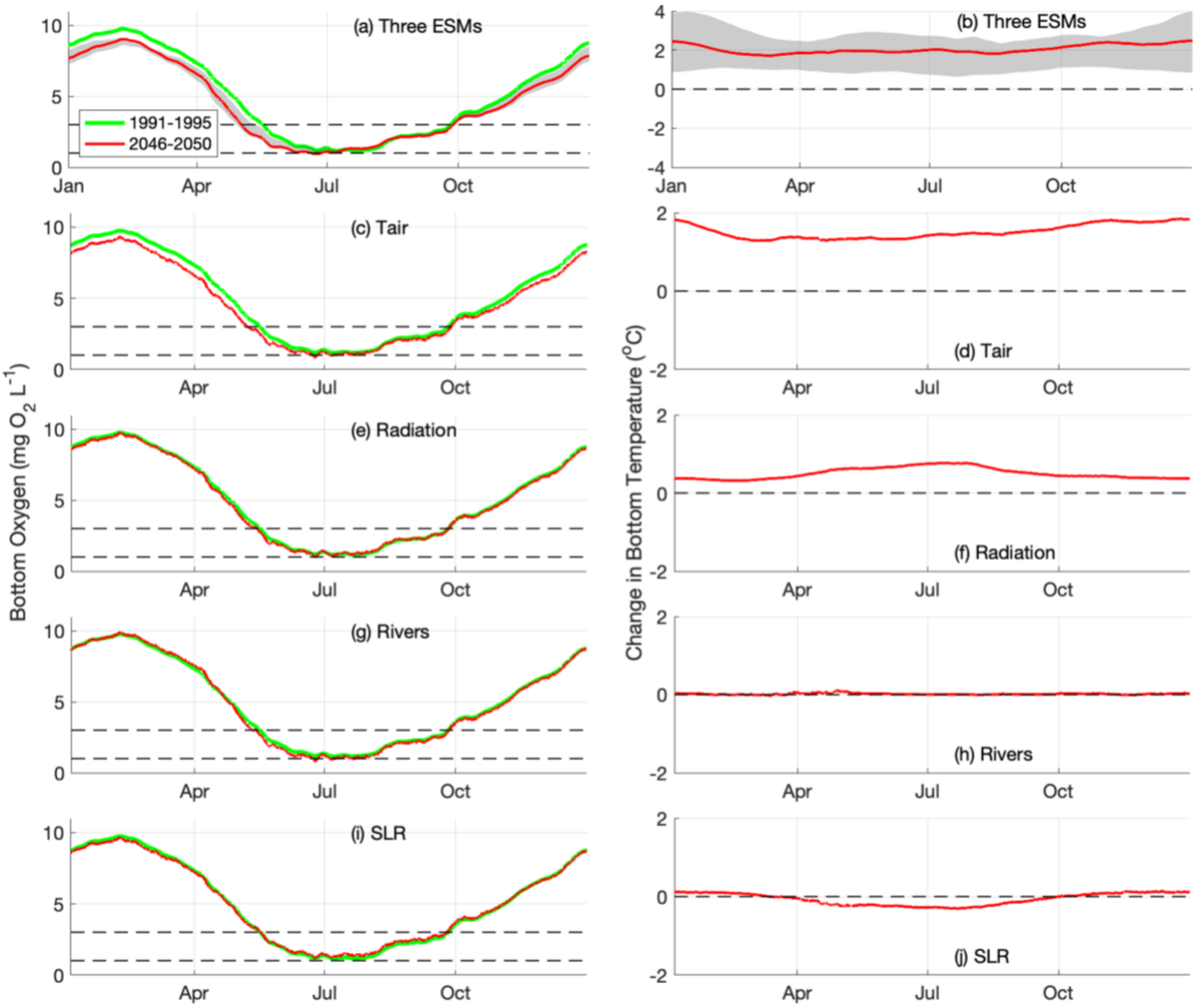


**Figure 5.** Modeled bottom $O_2$ and change in bottom temperature averaged over five years and nine CBP WQMP station locations (white stars in Fig. 1). Bottom $O_2$ is shown for the 1991-1995 Reference simulation (green line), and both bottom $O_2$ and change in bottom temperature (2046-2050 minus 1991-1995) is shown for the (a, b) median of the three future ESM runs, (c, d) $T_{air}$ run, (e, f) Radiation run, (g, h) Rivers run, and the (i, j) SLR run. The grey shaded areas are the range of the three future ESM runs. Dashed lines denote either $O_2$ thresholds of 1 mg $L^{-1}$ and 3 mg $L^{-1}$ or no change in bottom temperature.

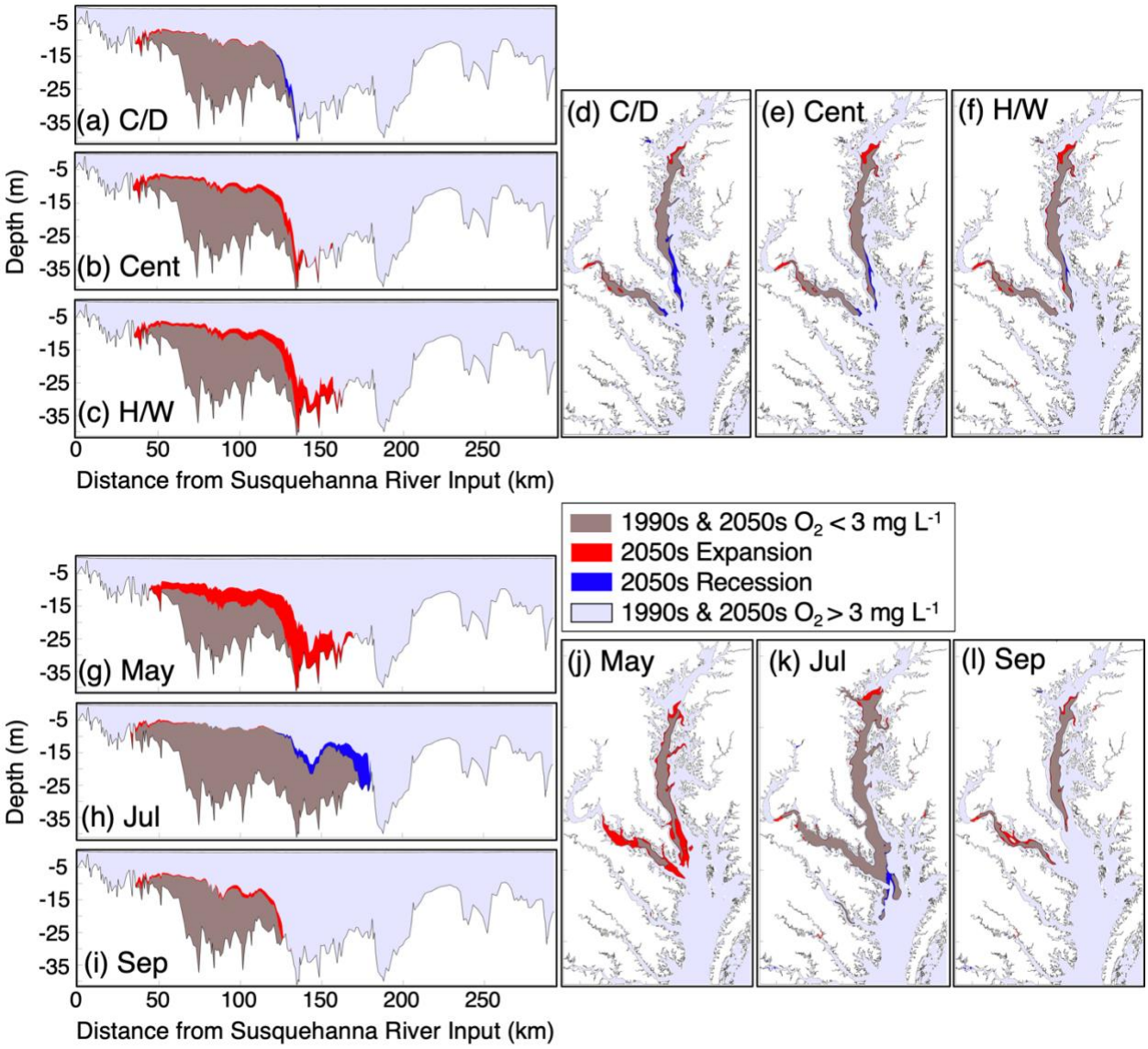


**Figure 6.** Modeled hypoxia ($O_2$ < 3 mg $L^{-1}$) in the Reference simulation and the three future ESM runs shown in top-down sections and downstream transects. Grey shading denotes hypoxia in both 1991-1995 and future; while red shading denotes expansion of hypoxia in the future runs, and blue shading represents locations where hypoxia does not exist in the future. Panels depict (a-f) hypoxia from each future run averaged over five years for the months of May-Oct, or (g-l) hypoxia averaged over the three future runs for five-year one-monthly averages of May, July, or September.

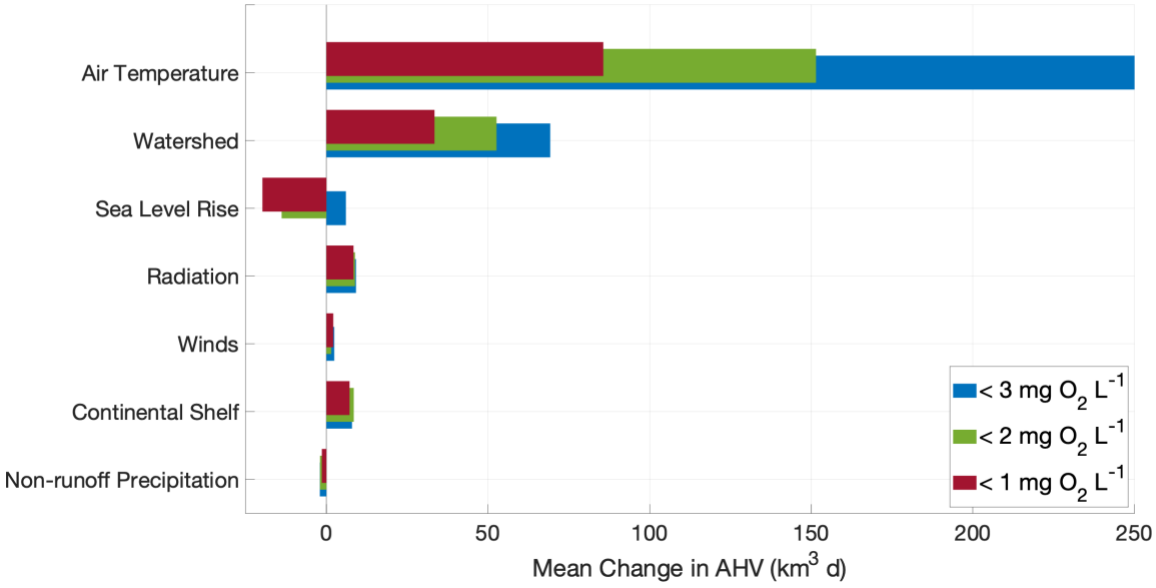


**Figure 7.** Five-year averaged change (2046-2050 minus 1991-1995) in annual hypoxic volume (AHV) of the climate variable runs. Bar color indicates $O_2$ threshold below which water is consider hypoxic.

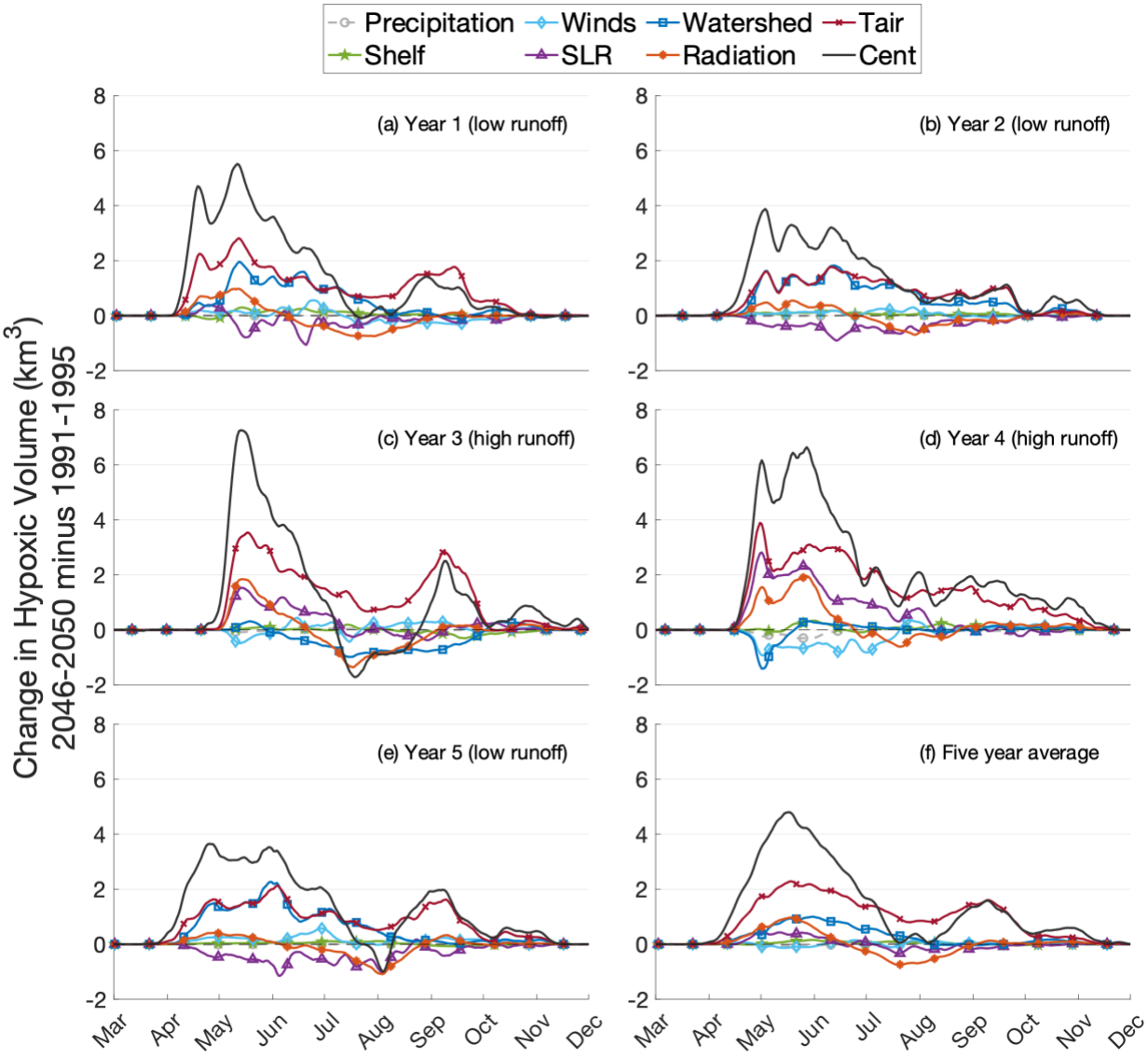


**Figure 8.** Change in daily hypoxic volume for $O_2 < 3$ mg $L^{-1}$, from March 1st to December 1st, in each climate variable run and the Centroid (Cent) run, (a-e) for each year and (f) averaged over all five years.

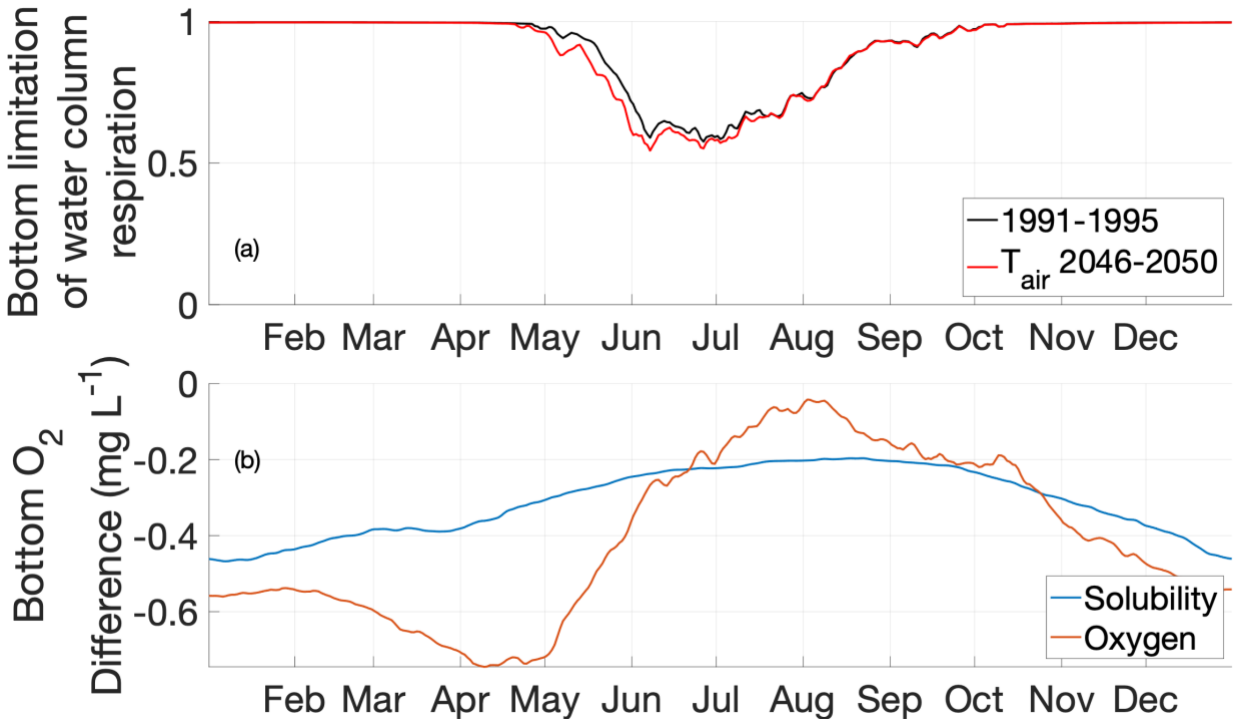


**Figure 9.** Timeseries of model output are averaged, over five years and nine CBP WQMP station locations, for bottom values of (a) modeled $O_2$ limitation of respiration in the 1991-1995 Reference simulation and $T_{air}$ run and (b) changes in $O_2$ solubility and actual concentration as the 2046-2050 $T_{air}$ run minus the 1991-1995 Reference simulation.

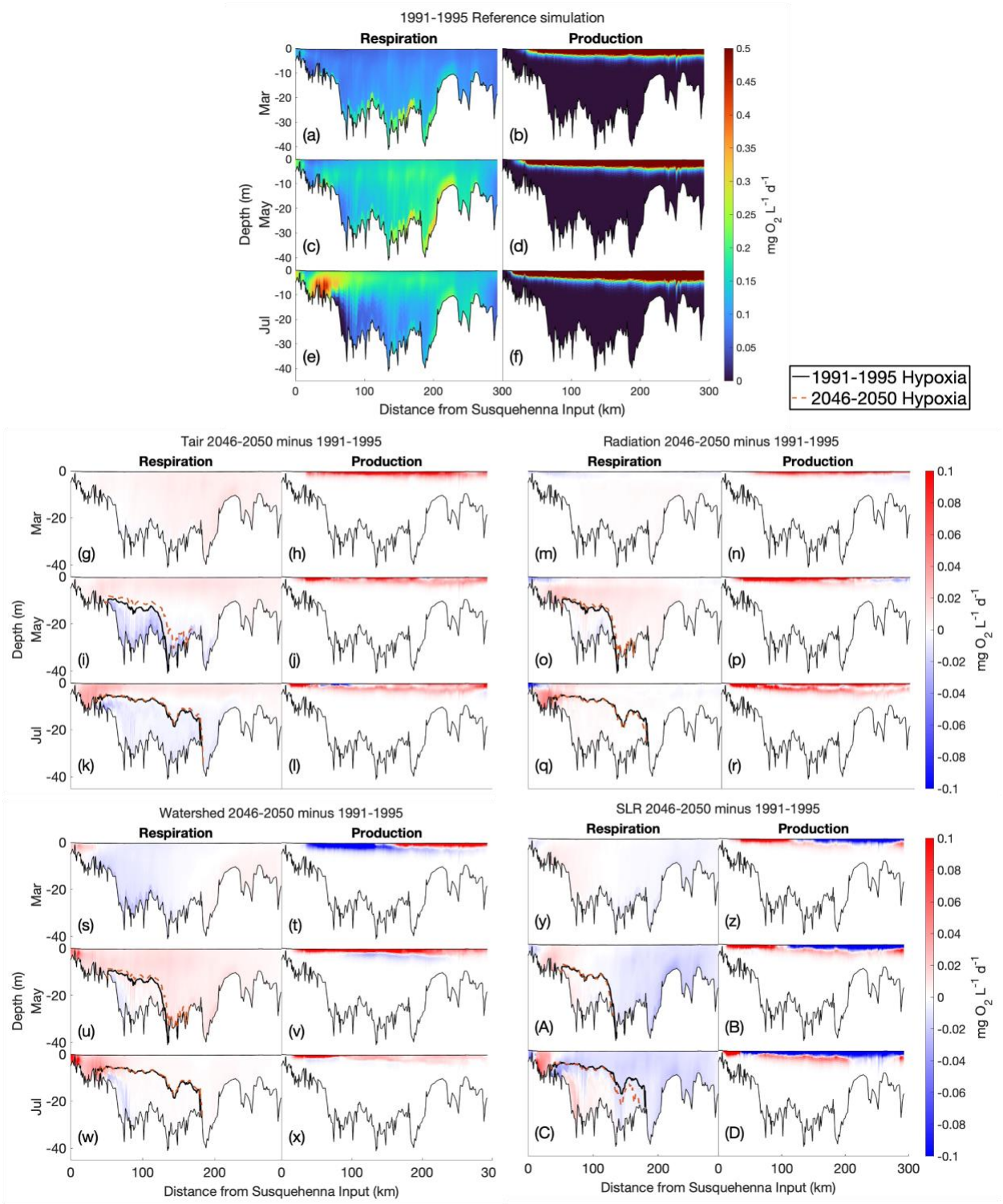


**Figure 10.** Production and respiration ($O_2$ fluxes) in ROMS-ECB for five-year averaged months March, May, and July. Panels depict (a-f) the 1991-1995 Reference simulation, the change (2046-2050 minus 1991-1995) in the (g-l) $T_{air}$ run, (m-r) Radiation run, (s-x) Watershed run, and (y-D) SLR run.

# SUPPLEMENTARY MATERIALS

**Table S1.** Change in AHV (for $O_2$ < 3 mg $L^{-1}$) between 1991-1995 (listed in Table 3) and the Centroid run as well as climate variable runs.

| Model Runs | Change in AHV ($km^3$ d) (2046-2050 minus 1991-1995) | | | | | |
|---|---|---|---|---|---|---|
| | Year 1 (Low runoff) | Year 2 (Low runoff) | Year 3 (High runoff) | Year 4 (High runoff) | Year 5 (Low runoff) | Average ± Standard Deviation |
| Centroid | 352 | 301 | 278 | 512 | 335 | 355 ± 92 |
| $T_{air}$ | 246 | 179 | 277 | 338 | 212 | 251 ± 61 |
| Watershed | 115 | 151 | -63 | -4 | 148 | 69 ± 97 |
| SLR | -32 | -61 | 56 | 145 | -78 | 6 ± 93 |
| Radiation | -6 | -4 | 2 | 65 | -13 | 9 ± 32 |
| Shelf | 14 | 11 | -6 | 16 | 5 | 8 ± 9 |
| Winds | -5 | 13 | 10 | -39 | 34 | 2 ± 27 |
| Precip | 1 | 1 | 0 | -12 | 0 | -2 ± 5.6 |

**Table S2.** Five-year averaged AHV for the three future ESM runs, Centroid, Hot/Wet (H/W) and Cool/Dry (C/D) and increases in AHV between 1991-1995 (listed in Table 3) and the climate variable runs.

| Model Runs | 2046-2050 AHV ($km^3$ d) | | Increase in AHV ($km^3$ d) (2046-2050 minus 1991-1995) | |
|---|---|---|---|---|
| | < 2 mg $O_2$ $L^{-1}$ | < 4 mg $O_2$ $L^{-1}$ | < 2 mg $O_2$ $L^{-1}$ | < 4 mg $O_2$ $L^{-1}$ |
| Centroid | 1128 ± 491 | 2951 ± 798 | 211 ± 81 | 591 ± 91 |
| C/D | 937 ± 431 | 2528 ± 751 | 21 ± 69 | 168 ± 105 |
| H/W | 1227 ± 485 | 3227 ± 757 | 311 ± 60 | 866 ± 94 |
| $T_{air}$ | 1068 ± 506 | 2752 ± 801 | 151 ± 55 | 392 ± 67 |
| Watershed | 969 ± 393 | 2440 ± 622 | 53 ± 69 | 79 ± 120 |
| SLR | 902 ± 504 | 2413 ± 873 | -14 ± 54 | 52 ± 137 |
| Radiation | 925 ± 476 | 2374 ± 760 | 9 ± 27 | 14 ± 32 |
| Shelf | 925 ± 459 | 2366 ± 735 | 8 ± 6 | 6 ± 11 |
| Winds | 918 ± 443 | 2365 ± 717 | 1 ± 21 | 5 ± 39 |
| Precip | 914 ± 455 | 2359 ± 738 | -2 ± 5 | -1 ± 5 |

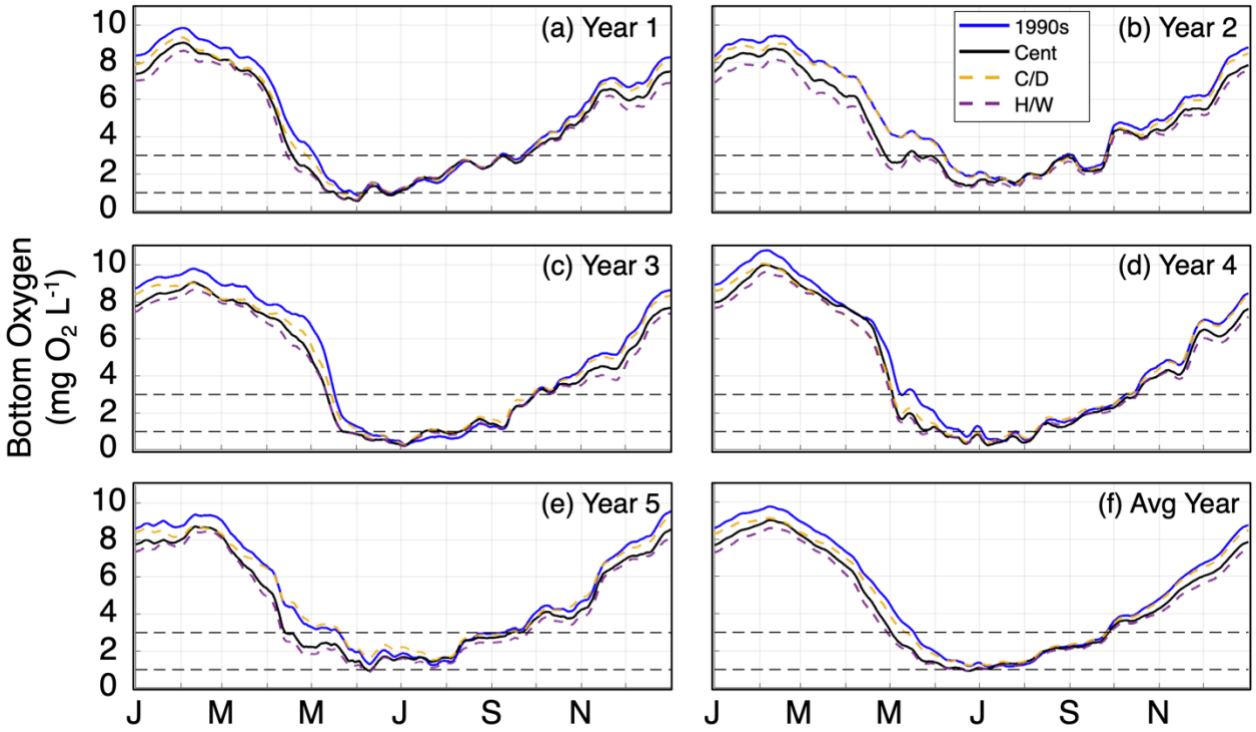


**Figure S1.** Modeled bottom $O_2$ averaged over five years and nine CBP WQMP station locations (white stars in Fig. 1) for Reference (blue line) and the three future ESM runs. Black dashed lines denote $O_2$ thresholds of 1 mg/L and 3 mg/L.

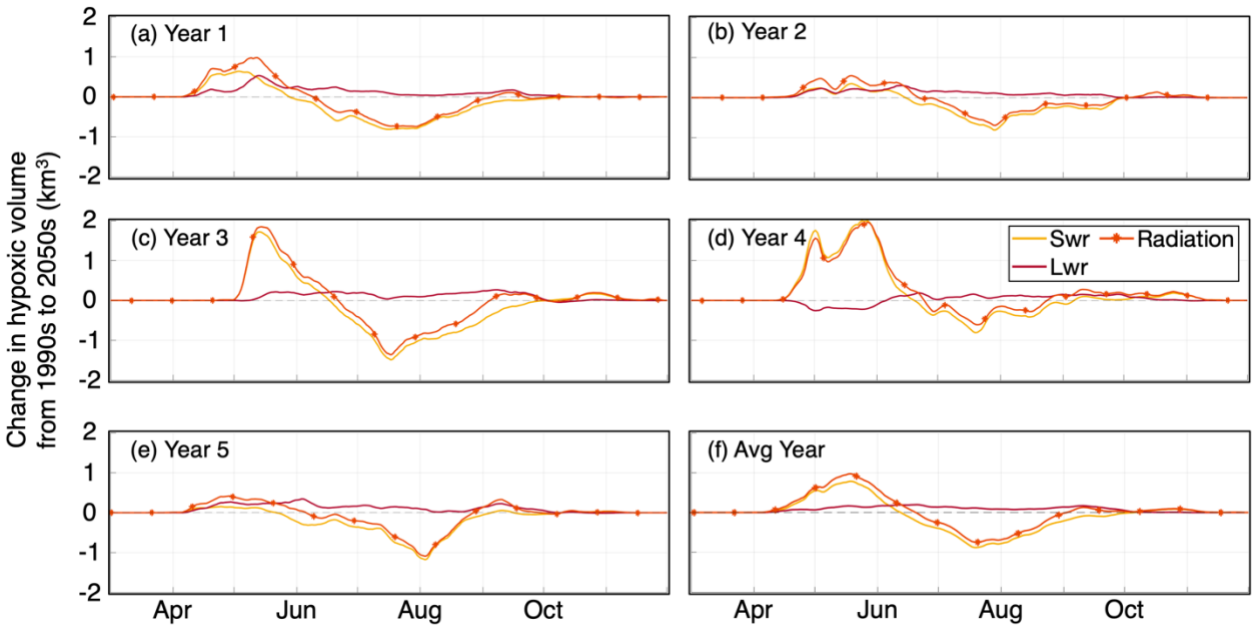


**Figure S2.** Change in daily hypoxic volume (2046-2050 minus 1991-1995), from March 1st to December 1st, in the Shortwave (Swr), Longwave (Lwr), and Radiation runs, (a-e) for each year and (f) averaged over all five years.

# REFERENCES


Abatzoglou, J. T. and Brown, T. J.: A comparison of statistical downscaling methods suited for wildfire applications, Int. J. Climatol., 32, 772–780, https://doi.org/10.1002/joc.2312, 2012.

Bever, A. J., Friedrichs, M. A. M., Friedrichs, C. T., Scully, M. E., and Lanerolle, L. W. J.: Combining observations and numerical model results to improve estimates of hypoxic volume within the Chesapeake Bay, USA: Improving Hypoxic Volume Estimates, J. Geophys. Res. Oceans, 118, 4924–4944, https://doi.org/10.1002/jgrc.20331, 2013.

Bever, A. J., Friedrichs, M. A. M., Friedrichs, C. T., and Scully, M. E.: Estimating hypoxic volume in the Chesapeake Bay using two continuously sampled oxygen profiles, J. Geophys. Res. Oceans, 123, 6392–6407, https://doi.org/10.1029/2018JC014129, 2018.

Bhatt, G., Linker, L., Shenk, G., Bertani, I., Tian, R., Rigelman, J., Hinson, K., and Claggett, P.: Water quality impacts of climate change, land use, and population growth in the Chesapeake Bay watershed, JAWRA J. Am. Water Resour. Assoc., https://doi.org/10.1111/1752-1688.13144, 2023.

Bianchi, T. S., DiMarco, S. F., Cowan, J. H., Hetland, R. D., Chapman, P., Day, J. W., and Allison, M. A.: The science of hypoxia in the Northern Gulf of Mexico: A review, Sci. Total Environ., 408, 1471–1484, https://doi.org/10.1016/j.scitotenv.2009.11.047, 2010.

Boon, J. D. and Mitchell, M.: Anthropocene sea level change: a history of recent trends observed in the U.S. east, gulf, and west coast regions, https://doi.org/10.21220/V5T17T, 2018.

Breitburg, D.: Effects of hypoxia, and the balance between hypoxia and enrichment, on coastal fishes and fisheries, Estuaries, 25, 767–781, https://doi.org/10.1007/BF02804904, 2002.

Cai, X., Shen, J., Zhang, Y. J., Qin, Q., Wang, Z., and Wang, H.: Impacts of sea-level rise on hypoxia and phytoplankton production in Chesapeake Bay: model prediction and assessment, J. Am. Water Resour. Assoc., 58, 922–939, https://doi.org/10.1111/1752-1688.12921, 2022.

Carstensen, J., Conley, D. J., Bonsdorff, E., Gustafsson, B. G., Hietanen, S., Janas, U., Jilbert, T., Maximov, A., Norkko, A., Norkko, J., Reed, D. C., Slomp, C. P., Timmermann, K., and Voss, M.: Hypoxia in the Baltic Sea: Biogeochemical Cycles, Benthic Fauna, and Management, AMBIO, 43, 26–36, https://doi.org/10.1007/s13280-013-0474-7, 2014.

CBP Database: https://www.chesapeakebay.net/what/downloads/cbp-water-quality-database-1984-present, last access: 8 January 2024.

Crear, D. P., Watkins, B. E., Friedrichs, M. A. M., St-Laurent, P., and Weng, K. C.: Estimating shifts in phenology and habitat use of cobia in Chesapeake Bay under climate change, Front. Mar. Sci., 7, 579135, https://doi.org/10.3389/fmars.2020.579135, 2020.

Da, F., Friedrichs, M. A. M., and St-Laurent, P.: Impacts of atmospheric nitrogen deposition and coastal nitrogen fluxes on oxygen concentrations in Chesapeake Bay, J. Geophys. Res. Oceans, 123, 5004–5025, https://doi.org/10.1029/2018JC014009, 2018.

Da, F., Friedrichs, M. A. M., St-Laurent, P., Shadwick, E. H., Najjar, R. G., and Hinson, K. E.: Mechanisms driving decadal changes in the carbonate system of a coastal plain estuary, J. Geophys. Res. Oceans, 126, https://doi.org/10.1029/2021JC017239, 2021.

Diaz, R. J. and Rosenberg, R.: Spreading dead zones and consequences for marine ecosystems, Science, 321, 926–929, https://doi.org/10.1126/science.1156401, 2008.

Dufresne, J.-L., Foujols, M.-A., Denvil, S., Caubel, A., Marti, O., Aumont, O., Balkanski, Y., Bekki, S., Bellenger, H., Benshila, R., Bony, S., Bopp, L., Braconnot, P., Brockmann, P., Cadule, P., Cheruy, F., Codron, F., Cozic, A., Cugnet, D., de Noblet, N., Duvel, J.-P., Ethé, C., Fairhead, L., Fichefet, T., Flavoni, S., Friedlingstein, P., Grandpeix, J.-Y., Guez, L., Guilyardi, E., Hauglustaine, D., Hourdin, F., Idelkadi, A., Ghattas, J., Joussaume, S., Kageyama, M., Krinner, G., Labetoulle, S., Lahellec, A., Lefebvre, M.-P., Lefevre, F., Levy, C., Li, Z. X., Lloyd, J., Lott, F., Madec, G., Mancip, M., Marchand, M., Masson, S., Meurdesoif, Y., Mignot, J., Musat, I., Parouty, S., Polcher, J., Rio, C., Schulz, M., Swingedouw, D., Szopa, S., Talandier, C., Terray, P., Viovy, N., and Vuichard, N.: Climate change projections using the IPSL-CM5 earth system model: from CMIP3 to CMIP5, Clim. Dyn., 40, 2123–2165, https://doi.org/10.1007/s00382-012-1636-1, 2013.

Duvall, M. S., Jarvis, B. M., and Wan, Y.: Impacts of climate change on estuarine stratification and implications for hypoxia within a shallow subtropical system, Estuar. Coast. Shelf Sci., 279, 108146, https://doi.org/10.1016/j.ecss.2022.108146, 2022.

Feng, Y., Friedrichs, M. A. M., Wilkin, J., Tian, H., Yang, Q., Hofmann, E. E., Wiggert, J. D., and Hood, R. R.: Chesapeake Bay nitrogen fluxes derived from a land-estuarine ocean biogeochemical modeling system: Model description, evaluation, and nitrogen budgets, J. Geophys. Res. Biogeosciences, 120, 1666–1695, https://doi.org/10.1002/2015JG002931, 2015.

Frankel, L. T., Friedrichs, M. A. M., St-Laurent, P., Bever, A. J., Lipcius, R. N., Bhatt, G., and Shenk, G. W.: Nitrogen reductions have decreased hypoxia in the Chesapeake Bay: evidence from empirical and numerical modeling, Sci. Total Environ., 814, 152722, https://doi.org/10.1016/j.scitotenv.2021.152722, 2022.

Garcia, H. E. and Gordon, L. I.: Oxygen solubility in seawater: Better fitting equations, Limnol. Oceanogr., 37, 1307–1312, https://doi.org/10.4319/lo.1992.37.6.1307, 1992.

Hafeez, M. A., Nakamura, Y., Suzuki, T., Inoue, T., Matsuzaki, Y., Wang, K., and Moiz, A.: Integration of weather research and forecasting (WRF) model with regional coastal ecosystem model to simulate the hypoxic conditions, Sci. Total Environ., 771, 145290, https://doi.org/10.1016/j.scitotenv.2021.145290, 2021.

Hao, L., Sanada, A., Chi, B., Xiong, B., Maruya, Y., and Yano, S.: Long-term developments in seasonal hypoxia and response to climate change: A three-decade modeling study in the Ariake

Sea, Japan, Sci. Total Environ., 929, 172471, https://doi.org/10.1016/j.scitotenv.2024.172471, 2024.

Hedges, K. J. and Abrahams, M. V.: Hypoxic refuges, predator–prey interactions and habitat selection by fishes, J. Fish Biol., 86, 288–303, https://doi.org/10.1111/jfb.12585, 2015.

Herrmann, M. and Najjar, R.: Strategy for estimating downwelling long wave radiation from air temperature, shortwave radiation, and humidity for the CHAMP project, ScholarSphere, https://doi.org/10.26207/4vm0-qk03, 2023.

Hersbach, H., Bell, B., Berrisford, P., Hirahara, S., Horányi, A., Muñoz-Sabater, J., Nicolas, J., Peubey, C., Radu, R., Schepers, D., Simmons, A., Soci, C., Abdalla, S., Abellan, X., Balsamo, G., Bechtold, P., Biavati, G., Bidlot, J., Bonavita, M., De Chiara, G., Dahlgren, P., Dee, D., Diamantakis, M., Dragani, R., Flemming, J., Forbes, R., Fuentes, M., Geer, A., Haimberger, L., Healy, S., Hogan, R. J., Hólm, E., Janisková, M., Keeley, S., Laloyaux, P., Lopez, P., Lupu, C., Radnoti, G., de Rosnay, P., Rozum, I., Vamborg, F., Villaume, S., and Thépaut, J.-N.: The ERA5 global reanalysis, Q. J. R. Meteorol. Soc., 146, 1999–2049, https://doi.org/10.1002/qj.3803, 2020.

Hinson, K. E.: Impacts and uncertainties of climate change on the Chesapeake Bay, Dissertation, The College of William and Mary, Williamsburg, Virginia, 2023.

Hinson, K. E., Friedrichs, M. A. M., St-Laurent, P., Da, F., and Najjar, R. G.: Extent and causes of Chesapeake Bay warming, J. Am. Water Resour. Assoc., 58, 805–825, https://doi.org/10.1111/1752-1688.12916, 2022.

Hinson, K. E., Friedrichs, M. A. M., Najjar, R. G., Herrmann, M., Bian, Z., Bhatt, G., St-Laurent, P., Tian, H., and Shenk, G.: Impacts and uncertainties of climate-induced changes in watershed inputs on estuarine hypoxia, Biogeosciences, 20, 1937–1961, https://doi.org/10.5194/bg-20-1937-2023, 2023.

Hinson, K. E., Friedrichs, M. A. M., Najjar, R. G., Bian, Z., Herrmann, M., St-Laurent, P., and Tian, H.: Response of hypoxia to future climate change is sensitive to methodological assumptions, Sci. Rep., 14, 17544, https://doi.org/10.1038/s41598-024-68329-3, 2024.

Hong, B., Xue, H., Zhu, L., and Xu, H.: Climatic change of summer wind direction and its impact on hydrodynamic circulation in the Pearl River Estuary, J. Mar. Sci. Eng., 10, 842, https://doi.org/10.3390/jmse10070842, 2022.

Hood, R. R., Shenk, G. W., Dixon, R. L., Smith, S. M. C., Ball, W. P., Bash, J. O., Batiuk, R., Boomer, K., Brady, D. C., Cerco, C., Claggett, P., de Mutsert, K., Easton, Z. M., Elmore, A. J., Friedrichs, M. A. M., Harris, L. A., Ihde, T. F., Lacher, L., Li, L., Linker, L. C., Miller, A., Moriarty, J., Noe, G. B., Onyullo, G. E., Rose, K., Skalak, K., Tian, R., Veith, T. L., Wainger, L., Weller, D., and Zhang, Y. J.: The Chesapeake Bay program modeling system: overview and recommendations for future development, Ecol. Model., 456, 109635, https://doi.org/10.1016/j.ecolmodel.2021.109635, 2021.

Hopkinson, C. S. and Vallino, J. J.: Efficient export of carbon to the deep ocean through dissolved organic matter, Nature, 433, 142–145, https://doi.org/10.1038/nature03191, 2005.

Hopkinson, C. S., Buffam, I., Hobbie, J., Vallino, J., Perdue, M., Eversmeyer, B., Prahl, F., Covert, J., Hodson, R., Moran, M. A., Smith, E., Baross, J., Crump, B., Findlay, S., and Foreman, K.: Terrestrial inputs of organic matter to coastal ecosystems: An intercomparison of chemical characteristics and bioavailability, Biogeochemistry, 43, 211–234, https://doi.org/10.1023/A:1006016030299, 1998.

Huggett, R. D., Haigh, I. D., and Purdie, D. A.: Modelling the impact of river flow, macronutrients and solar radiation on the eutrophication status of small shallow estuaries, J. Mar. Syst., 222, 103606, https://doi.org/10.1016/j.jmarsys.2021.103606, 2021.

Irby, I. D., Friedrichs, M. A. M., Da, F., and Hinson, K. E.: The competing impacts of climate change and nutrient reductions on dissolved oxygen in Chesapeake Bay, Biogeosciences, 15, 2649–2668, https://doi.org/10.5194/bg-15-2649-2018, 2018.

Katsavounidis, I., Jay Kuo, C.-C., and Zhen Zhang: A new initialization technique for generalized Lloyd iteration, IEEE Signal Process. Lett., 1, 144–146, https://doi.org/10.1109/97.329844, 1994.

Kemp, W., Boynton, W., Adolf, J., Boesch, D., Boicourt, W., Brush, G., Cornwell, J., Fisher, T., Glibert, P., Hagy, J., Harding, L., Houde, E., Kimmel, D., Miller, W., Newell, R., Roman, M., Smith, E., and Stevenson, J.: Eutrophication of Chesapeake Bay: historical trends and ecological interactions, Mar. Ecol. Prog. Ser., 303, 1–29, https://doi.org/10.3354/meps303001, 2005.

Leal Filho, W., Nagy, G. J., Martinho, F., Saroar, M., Erache, M. G., Primo, A. L., Pardal, M. A., and Li, C.: Influences of climate change and variability on estuarine ecosystems: an impact study in selected European, South American and Asian countries, Int. J. Environ. Res. Public. Health, 19, 585, https://doi.org/10.3390/ijerph19010585, 2022.

Linker, L. C., Shenk, G. W., Bhatt, G., Tian, R., Cerco, C. F., and Bertani, I.: Simulating climate change in a coastal watershed with an integrated suite of airshed, watershed, and estuary models, JAWRA J. Am. Water Resour. Assoc., 60, 499–528, https://doi.org/10.1111/1752-1688.13185, 2024.

Luettich, R. A. (Richard A., Westerink, J. J., and Scheffner, N. W.: ADCIRC : an advanced three-dimensional circulation model for shelves, coasts, and estuaries. Report 1, Theory and methodology of ADCIRC-2DD1 and ADCIRC-3DL, This Digital Resource was created from scans of the Print Resource, Coastal Engineering Research Center (U.S.), 1992.

Martin, G. M., Bellouin, N., Collins, W. J., Culverwell, I. D., Halloran, P. R., Hardiman, S. C., Hinton, T. J., Jones, C. D., McDonald, R. E., McLaren, A. J., O'Connor, F. M., Roberts, M. J., Rodriguez, J. M., Woodward, S., Best, M. J., Brooks, M. E., Brown, A. R., Butchart, N., Dearden, C., Derbyshire, S. H., Dharssi, I., Doutriaux-Boucher, M., Edwards, J. M., Falloon, P. D., Gedney, N., Gray, L. J., Hewitt, H. T., Hobson, M., Huddleston, M. R., Hughes, J., Ineson, S., Ingram, W. J., James, P. M., Johns, T. C., Johnson, C. E., Jones, A., Jones, C. P., Joshi, M. M., Keen, A. B., Liddicoat, S., Lock, A. P., Maidens, A. V., Manners, J. C., Milton, S. F., Rae, J.

G. L., Ridley, J. K., Sellar, A., Senior, C. A., Totterdell, I. J., Verhoef, A., Vidale, P. L., and Wiltshire, A.: The HadGEM2 family of Met Office unified model climate configurations, Geosci. Model Dev., 4, 723–757, https://doi.org/10.5194/gmd-4-723-2011, 2011.

McCrackin, M. L., Jones, H. P., Jones, P. C., and Moreno-Mateos, D.: Recovery of lakes and coastal marine ecosystems from eutrophication: A global meta-analysis, Limnol. Oceanogr., 62, 507–518, https://doi.org/10.1002/lno.10441, 2017.

Meier, H. E. M., Edman, M., Eilola, K., Placke, M., Neumann, T., Andersson, H. C., Brunnabend, S.-E., Dieterich, C., Frauen, C., Friedland, R., Gröger, M., Gustafsson, B. G., Gustafsson, E., Isaev, A., Kniebusch, M., Kuznetsov, I., Müller-Karulis, B., Naumann, M., Omstedt, A., Ryabchenko, V., Saraiva, S., and Savchuk, O. P.: Assessment of uncertainties in scenario simulations of biogeochemical cycles in the Baltic Sea, Front. Mar. Sci., 6, 46, https://doi.org/10.3389/fmars.2019.00046, 2019.

Meier, H. E. M., Dieterich, C., and Gröger, M.: Natural variability is a large source of uncertainty in future projections of hypoxia in the Baltic Sea, Commun. Earth Environ., 2, 50, https://doi.org/10.1038/s43247-021-00115-9, 2021.

Moss, R. H., Edmonds, J. A., Hibbard, K. A., Manning, M. R., Rose, S. K., Van Vuuren, D. P., Carter, T. R., Emori, S., Kainuma, M., Kram, T., Meehl, G. A., Mitchell, J. F. B., Nakicenovic, N., Riahi, K., Smith, S. J., Stouffer, R. J., Thomson, A. M., Weyant, J. P., and Wilbanks, T. J.: The next generation of scenarios for climate change research and assessment, Nature, 463, 747–756, https://doi.org/10.1038/nature08823, 2010.

Ni, W. and Li, M.: What drove the nonlinear hypoxia response to nutrient loading in Chesapeake Bay during the 20th century?, Sci. Total Environ., 861, 160650, https://doi.org/10.1016/j.scitotenv.2022.160650, 2023.

Ni, W., Li, M., Ross, A. C., and Najjar, R. G.: Large projected decline in dissolved oxygen in a eutrophic estuary due to climate change, J. Geophys. Res. Oceans, 124, 8271–8289, https://doi.org/10.1029/2019JC015274, 2019.

Ni, W., Li, M., and Testa, J. M.: Discerning effects of warming, sea level rise and nutrient management on long-term hypoxia trends in Chesapeake Bay, Sci. Total Environ., 737, 139717, https://doi.org/10.1016/j.scitotenv.2020.139717, 2020.

Redfield, A. C.: On the proportions of organic derivatives in sea water and their relation to the composition of plankton, 1934.

Scully, M. E.: Wind modulation of dissolved oxygen in Chesapeake Bay, Estuaries Coasts, 33, 1164–1175, https://doi.org/10.1007/s12237-010-9319-9, 2010.

Scully, M. E.: Mixing of dissolved oxygen in Chesapeake Bay driven by the interaction between wind-driven circulation and estuarine bathymetry, J. Geophys. Res. Oceans, 121, 5639–5654, https://doi.org/10.1002/2016JC011924, 2016a.

Scully, M. E.: The contribution of physical processes to inter-annual variations of hypoxia in Chesapeake Bay: a 30-yr modeling study, Limnol. Oceanogr., 61, 2243–2260, https://doi.org/10.1002/lno.10372, 2016b.

Scully, M. E., Geyer, W. R., Borkman, D., Pugh, T. L., Costa, A., and Nichols, O. C.: Unprecedented summer hypoxia in southern Cape Cod Bay: an ecological response to regional climate change?, Biogeosciences, 19, 3523–3536, https://doi.org/10.5194/bg-19-3523-2022, 2022.

Shchepetkin, A. F. and McWilliams, J. C.: The regional oceanic modeling system (ROMS): a split-explicit, free-surface, topography-following-coordinate oceanic model, Ocean Model., 9, 347–404, https://doi.org/10.1016/j.ocemod.2004.08.002, 2005.

Slesinger, E., Andres, A., Young, R., Seibel, B., Saba, V., Phelan, B., Rosendale, J., Wieczorek, D., and Saba, G.: The effect of ocean warming on black sea bass (Centropristis striata) aerobic scope and hypoxia tolerance, PLOS ONE, 14, e0218390, https://doi.org/10.1371/journal.pone.0218390, 2019.

Staniec, A. and Vlahos, P.: Timescales for determining temperature and dissolved oxygen trends in the Long Island Sound (LIS) estuary, Cont. Shelf Res., 151, 1–7, https://doi.org/10.1016/j.csr.2017.09.013, 2017.

St-Laurent, P., Friedrichs, M. A. M., Li, M., and Ni, W.: Impacts of sea level rise on hypoxia in the Chesapeake Bay: a model intercomparison, Virginia Institute of Marine Science, William and Mary, 2019.

St-Laurent, P., Friedrichs, M. A. M., Najjar, R. G., Shadwick, E. H., Tian, H., and Yao, Y.: Relative impacts of global changes and regional watershed changes on the inorganic carbon balance of the Chesapeake Bay, Biogeosciences, 17, 3779–3796, https://doi.org/10.5194/bg-17-3779-2020, 2020.

Taylor, K. E., Stouffer, R. J., and Meehl, G. A.: An overview of CMIP5 and the experiment design, Bull. Am. Meteorol. Soc., 93, 485–498, https://doi.org/10.1175/BAMS-D-11-00094.1, 2012.

Tian, R., Cerco, C. F., Bhatt, G., Linker, L. C., and Shenk, G. W.: Mechanisms controlling climate warming impact on the occurrence of hypoxia in Chesapeake Bay, J. Am. Water Resour. Assoc., 58, 855–875, https://doi.org/10.1111/1752-1688.12907, 2022.

Tuckey, T. D. and Fabrizio, M. C.: Variability in fish tissue proximate composition is consistent with indirect effects of hypoxia in Chesapeake Bay tributaries, Mar. Coast. Fish., 8, 1–15, https://doi.org/10.1080/19425120.2015.1103824, 2016.

Turner, J. S., St-Laurent, P., Friedrichs, M. A. M., and Friedrichs, C. T.: Effects of reduced shoreline erosion on Chesapeake Bay water clarity, Sci. Total Environ., 769, 145157, https://doi.org/10.1016/j.scitotenv.2021.145157, 2021.

USEPA: Ambient water quality criteria for dissolved oxygen, water clarity and chlorophyll a for the Chesapeake Bay and Its tidal tributaries, U.S. Environmental Protection Agency Region III, Chesapeake Bay Program Office, Annapolis, MD, 2003.

Volodin, E. M., Dianskii, N. A., and Gusev, A. V.: Simulating present-day climate with the INMCM4.0 coupled model of the atmospheric and oceanic general circulations, Izv. Atmospheric Ocean. Phys., 46, 414–431, https://doi.org/10.1134/S000143381004002X, 2010.

Wang, P., Wang, H., and Linker, L.: Relative importance of nutrient load and wind on regulating interannual summer hypoxia in the Chesapeake Bay, Estuaries Coasts, 38, 1048–1061, https://doi.org/10.1007/s12237-014-9867-5, 2015.

Wang, P., Linker, L., Wang, H., Bhatt, G., Yactayo, G., Hinson, K., and Tian, R.: Assessing water quality of the Chesapeake Bay by the impact of sea level rise and warming, IOP Conf. Ser. Earth Environ. Sci., 82, 012001, https://doi.org/10.1088/1755-1315/82/1/012001, 2017.

Zweng, M., Reagan, J., Seidov, D., Boyer, T., Locarnini, M., Garcia, H., Mishonov, A., Baranova, O., Weathers, K., Paver, C., and Smolyar, I.: World ocean atlas 2018, volume 2: salinity, U.S. DEPARTMENT OF COMMERCE National Oceanic and Atmospheric Administration, Silver Spring, MD, 2019.